Modelling and Evaluation of Tension Type Flight Intersection Joint

Submitted in partial fulfilment of the requirements for the award of the degree of

Doctor of Philosophy

by

Masuram Umakanth
Roll No. 717024

Supervisors

Prof. Srikanth Korla, Mechanical Engineering, NIT Warangal
Dr. V. Narayanamurthy, Research Centre Imarat (DRDO), Hyderabad

Mechanical Engineering Department
NATIONAL INSTITUTE OF TECHNOLOGY WARANGAL
2022

Thesis approval for PhD

This Thesis entitled **"Modelling and Evaluation of Tension Type Flight Intersection Joint"** submitted by Mr. **Masuram Umakanth** is approved for the Degree of Doctor of Philosophy

Examiners

_____

_____

_____

Supervisors

Dr. Srikanth Korla

Dr. V. Narayanamurthy

Chairman

Prof. V. Suresh Babu
Date: _____

Abstract

Slender flight vehicles such as launch vehicles and missiles are thin-walled structures made of several airframe sections connected together using an appropriate flight intersection joint (FIJ). These FIJs help in easy assembly and disassembly of airframe sections for integration, maintenance and operational health checks of configured subsystems within the airframe sections. Several types of FIJs are commonly adopted in practice and the selection of a particular type depends upon the available volume, geometry, material, size and configuration of the flight airframe sections and the kind of joint stiffness acceptable to the flight. The FIJs are characterized by the joint rotational compliance (JRC) and the capability to withstand the flight, transportation and handling loads. Although different types of FIJs are found in practice and different literature, a comprehensive review on FIJs is unavailable. The JRC is an important parameter in the structural design and analysis of a launch vehicle, but there are no theoretical model to predict JRC of a FIJ, even the prediction by numerical methods is not yet well matured, it is always experimentally determined for a given type of FIJ, and further there is no clarity on number and size of fasteners to be adopted for achieving a required JRC for a FIJ. This research on FIJ is attempted to address these limitations.

The first phase of the research brings out a comprehensive review of the FIJs. This review, in detail, covers the classification of intersection joints, different loads experienced by the joints, and predictive and experimental methods adopted in the determination of JRC and its importance in predicting the dynamics of a flight vehicle. The JRC is always quantified through extensive experiments due to non-availability of a reliable theoretical or numerical model. In the second phase of research, an analytical model is derived based on localised component joint stiffness wherein the latter is modelled and quantified through numerical methods, and verified through experiments. In the third phase, the analytically predicted JRC for a typical FIJ is compared with JRC obtained from an independent numerical modelling of the full FIJ based on finite element analysis (FEA), wherein a very good agreement is observed. Further, the effect of pre-tightening of studs, variations in size and number of studs and their combinations and joint's geometric parameters on JRC of a FIJ are investigated. It has been demonstrated that (1) the pre-tightening of studs enhances the JRC to an extent of 30% to 10% when loading is increased respectively from no load to the first yield moment; and (2) the increase in number of studs for a given stud size result in significantly enhanced JRC as compared to the increase in size of studs.

In the fourth phase, an experimental setup is designed and analysed through FEA under bending moments up to 20% of the airframe's first yield moment for design applications. Four numbers of FIJs are manufactured and experimented to determine the JRC. The experimentally measured JRC matched very well with analytical and numerical predictions, thereby validating the predictive model thus formulated and the adopted method of numerical simulation. Finally, in the fifth phase of research, effect of variation in diameter of FIJ on JRC is analyzed through FEA for three different cases viz. under a constant bending moment for all diameters, FIJs subjected up to respective first yield moment, and a FIJ with number of studs configured at constant arc length. This study brought out that the JRC reduces with increase in diameter of FIJ in the first case, exhibited almost similar performance in the second case for all diameters and shown a significant reduction in JRC in the third case with increase in diameter of FIJ.

As a whole, all five phases of research addressed in the thesis provided a reliable analytical model and a robust numerical simulation approach for determination of JRC of a FIJ, validated by experiments. Further, clarity on variation of important joint parameters is brought out. This research outcomes will certainly help address the design requirements of FIJs.

Declaration

This is to certify that the work presented in the thesis entitled **Modelling and Evaluation of Tension Type Flight Intersection Joint** is a bonafide work done by me under the supervision of Dr. Srikanth Korla and Dr. V. Narayanamurthy and was not submitted elsewhere for the award of any degree.

I declare that this written submission represents my ideas in my own words and where others' ideas or words have been included, I have adequately cited and referenced the original sources. I also declare that I have adhered to all principles of academic honesty and integrity and have not misrepresented or fabricated or falsified any idea / data / fact / source in my submission. I understand that any violation of the above will be a cause for disciplinary action by the Institute and can also evoke penal action from the sources which have thus not been properly cited or from whom proper permission has not been taken when needed.

_____

(Signature)

Masuram Umakanth

(Name of the student)

717024

(Roll No.)

Date: _____

Acknowledgement

I would like to offer my sincere gratitude to the Director, RCI and Shri. S. Gopinath, OS, RCI for giving me the opportunity to conduct Ph.D. research on modelling and evaluation of tension type flight intersection joint.

I am very thankful to Dr. Srikanth Korla, my thesis supervisor (Internal) who constantly guided me during the research and also taught the course on Engineering Design. His inputs were very useful during the research.

I am very grateful to Dr. Vijayabaskar Narayanamurthy, my thesis supervisor (External) who motivated, encouraged, and provided a detailed guidance in conceptualizing and formulating the problem and carrying out experiments.

My special gratitude to the DSC members Prof. A. Venugopal, Prof. V. Suresh Babu from MED and Shri T.P. Tezeswi, Assoc. Prof. CED for their valuable suggestions and improvements during the entire research period.

I take this opportunity to thank friends from DRDL-Material Testing Division for facilitating in conduct of experiments on test specimens and local joints; and the ENTEST team at RCI for supporting me in establishing the magnanimous test setup and conduct of full-scale experiments on FIJs.

I wish to thank Shri P. Uday Kumar, Engineer for his support in FEA and experiments. I express my gratitude to the assistance provided by Shri. A. Srikanth, and Shri. G. Ramesh for integration of experimental setup and in carrying out the experiments.

I specially thank my wife Smt. Savitha, and my daughters Vakshika and Gayatri for their constant support and encouragement in my career progress. Especially, I express my gratitude to my father Shri M. Venkateshwar Rao and mother Smt. M. Sugandhamala, for their blessings.

Masuram Umakanth

Table of Contents

List of Figures

List of Tables

List of Symbols

a	:	Distance from airframe center to neutral axis
b	:	Bolt spacing
C	:	Joint flexural compliance
d	:	Diameter of bolt
D_f	:	Diameter of flange
D_p	:	Pitch circle diameter of bolts
D	:	Diameter of the tube
E_p	:	Modulus of elasticity of plate
E_b	:	Modulus of elasticity of bolt
E_iI_i	:	Flexural rigidity
FIJ	:	Flight Intersection Joint
F_C	:	Forces on compression side
F_T	:	Forces on tension side
F_{Cn}	:	Force in compression spring
F_{Tm}	:	Force in tension spring
F_i	:	Preload
F_w	:	Force due to wind
F_d	:	Force due to drag
k_b	:	Stiffness of bolt
k_m	:	Stiffness of members
k_c	:	Stiffness in compression spring
k_t	:	Stiffness in tension spring
m	:	Number of springs in tension
M	:	Bending moment
M_C	:	Resulting bending moment in compression
M_T	:	Resulting bending moment in tension
M_{Cm}	:	Bending moment in compression
M_{Ct}	:	Bending moment in tension
M_y	:	Bending moment at yield
M_e	:	Engine mass
M_a	:	Avionics mass
n	:	Number of springs in compression

N	:	Axial compressive force
PCD	:	Pitch Circle Diameter
q	:	Dynamic pressure
r	:	Distance from airframe to stud center
RB	:	Reference bottom
RL	:	Reference left
RR	:	Reference right
RT	:	Reference top
R_T	:	Resistance in Tension
R_C	:	Resistance in Compression
S	:	Joint stiffness
t	:	Plate thickness
T	:	Tension force
T_{RM}	:	Thrust force from rocket motor
T_{bo}	:	Total bolt preload
U_b	:	Strain energy in bolt
U_m	:	Strain energy in members
UTM	:	Universal Testing Machine
u_{tm}	:	Displacement of springs in tension
u_{cn}	:	Displacement of springs in compression
W	:	Self-weight of launch vehicle
X_g	:	Centre of gravity
x_p	:	Centre of pressure
y_{tm}	:	Distance from stud axis to neutral axis in tension
y_{cn}	:	Distance from stud axis to neutral axis in compression
Z	:	Ratio of bending stiffness of bolt to plate bearing stiffness
z	:	Spacing of bolts
ϕ	:	Rotation in radians
θ	:	Angle between stud axis to Reference top
v	:	Poisson's ratio
μ	:	Slope of the bolt force T_b versus the tension force T
δ	:	Deflection
δ_b	:	Deflection in bolt
δ_m	:	Deflection in members

Publications from Thesis

Peer Reviewed Journals

1. M. Umakanth, V. Narayanamurthy, S. Korla, A review of flight intersection joints, *International Journal of Reviews in Aerospace Engineering* (IREASE), 2021, 14(3): pp 131-148. https://doi.org/10.15866/irease.v14i3.19401.
2. M. Umakanth, P. Udaykumar, V. Narayanamurthy, S. Korla, Predicting the rotational compliance of a flight inter-section joint, *NMIMS Journal of Engineering and Technological Review,* 2021, 3(1): pp 62-73.
3. M. Umakanth, P. Udaykumar, V. Narayanamurthy, S. Korla, Influence of number of studs on compliance of a flight intersection joint, *IOP Conf. Series: Material Science and Engineering,* 2021, 1166: pp 1-8. doi:10.1088/1757-899X/1166/1/012050.
4. M. Umakanth, P. Udaykumar, V. Narayanamurthy, S. Korla, Axial stiffness of a slot-nut type conformal segment joint, *Recent Advances in Applied Mechanics*, Springer Nature, 2022: pp 367-377. https://doi.org/10.1007/978-981-16-9539-1_26.
5. M. Umakanth, P. Udaykumar, V. Narayanamurthy, S. Korla, Modelling the joint rotational compliance of stud and slot type inter-section joint, *Thin-Walled Structures*, Accepted. Manuscript Number: TWST-D-22-00224R1.

Peer Reviewed International and National Conferences

1. M. Umakanth, P. Udaykumar, V. Narayanamurthy, S. Korla, Rotational compliance of a flight inter-section joint, Proceedings of Virtual Seminar on Applied Mechanics, VSAM-2020, Aug 28, 2020.
2. M. Umakanth, P. Udaykumar, V. Narayanamurthy, S. Korla, Influence of number of studs on compliance of a flight intersection joint, Third Int. Conf. on Material Science and Manufacturing Technology, ICMSMT-2021, April 15-16, 2021.
3. M. Umakanth, P. Udaykumar, V. Narayanamurthy, S. Korla, Axial stiffness of a slot-nut type conformal segment joint, Proceedings of Virtual Seminar on Applied Mechanics, VSAM-2021, May 28, 2021.

Chapter-1

Introduction

1.1 Background

The launch vehicles and missiles are slender flight vehicles configured structurally by interconnection of several airframe sections as shown in Fig. 1.1. The airframe structural geometry is commonly made of cylindrical, ogival or conical. This interconnection between one airframe sections with another adjacent airframe section is achieved through intersection joints. Preferably, the flight intersection joints (FIJ) are conformal to the airframe's outer geometric profile without any external projections which in turn may cause aerodynamic drag. Mostly, the FIJs are temporary joints which can be opened or fastened on need. Only in certain uncommon cases, to meet the manufacturing and integration constraints, the airframe structural sections are made separately and then joined at intersections either permanently by welding or semi-permanently by riveting, Maloney *et al.* [1].

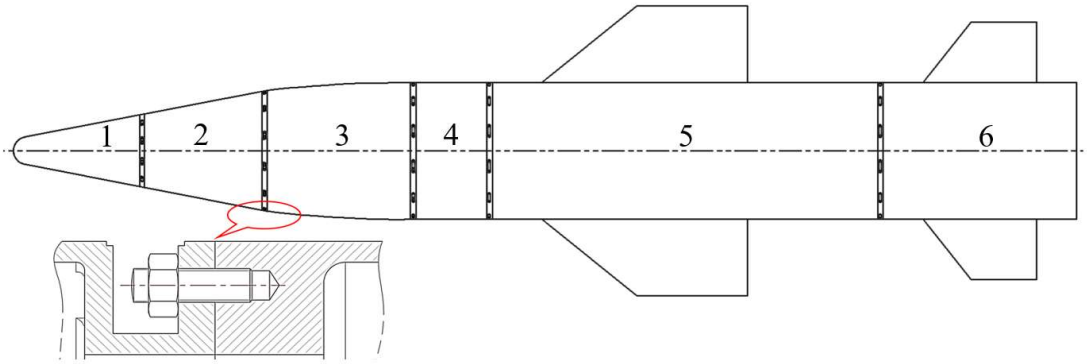

Fig. 1.1. Typical flight vehicle with five FIJs connecting six airframe sections [2]

Different subsystems intended to meet the configuration are generally mounted inside the airframe sections with in the available space. The FIJs, besides aiding in easy assembly and disassembly of subsystems, are also designed for easy integration and disintegration of one airframe section with another in a shorter time with minimal effort, employing standard tools. The design of FIJs is evolved with an emphasis to meet the functional and stiffness requirements.

Flight intersection joints experience more challenging requirements when compared to the bolted joints used in other engineering applications as they are exposed to more harsh environments during flight and operational readiness. Besides flight loads, they are also subjected to operational loads due to handling (i.e. lifting during loading and unloading), articulation (i.e. positioning from horizontal to vertical or at an inclination before launch) and transportation (through a launcher or a transporter). Several types of intersection joints are commonly adopted in practice and the selection of a particular type depends upon the available internal volume, geometry, material, size and configuration of the flight airframe sections, and the kind of joint stiffness, which has a vital impact on the global behaviour of the structure that is acceptable to the flight vehicle. The intersection joints are characterised by the joint compliance and the capability to withstand the flight, transportation and handling loads.

Although there are several types of flight intersection joints, their engineering design, constructional details and concepts are different from each other (Maloney et al. , Hillmer, Lasker et al. and Gharouni et al. 1-6). But their loadings and method of prediction of joint stiffness can be closely related to the mechanics of bolted circular flange joints adopted in tubular structures commonly found in general engineering applications. Significant research has been carried out for many years on bolted circular flange joints in tubular structures and different methods for the design of these joints have been developed. On the other hand, comparatively, the quantum of research on FIJs is very small and only limited knowledge is published in open literature. The design of FIJs relied more on meeting functional and stiffness requirements based on elaborate experiments and limited theoretical studies. But the well-established concepts and the method of analysis of bolted circular flange joints in tubular structures can be extended to develop the theoretical models and numerical analysis of FIJs. This background has driven the initiation of this thesis research.

1.2 Motivation and Research Gaps

1.2.1 Motivation

Considerable studies were carried out on predicting the joint compliance and clamping force distribution in bolted joints used in general engineering applications. These studies bought out simplified theoretical models, validated mostly by finite element analyses (FEA) and in few cases by experiments. There are few studies on bolted circular flange joints which provided methodologies for quantifying the joint stiffness and clamping force distribution (Rockey et al.

S. Igarashi et al., B. Kato et al., J.A. Packer et al. , J. J. Cao et al., G. Stamatopoulos at al. , M. Couchaux et al. , A. Kozlowski et al. , M.R. Azim et al. , M. Emara et al. , J. Kim et al., N. Rasti et al. , 7-37) The knowledge gained in the study of general engineering bolted joints and the bolted circular flange joints in tubular structures can be extended to study the mechanics of FIJs.

The quantification of JRC of FIJs have so far been governed by experimental techniques. Alley and his team [44-46] conducted experiments on 10 flight vehicles of different diameters and quantified JRC. They were the first in classifying FIJs based on JRC values *w.r.t.* variation in the diameter. They brought out an empirical relation between JRC (in radians/inch-pound) and diameter *D* (inch) of the flight vehicle as

$$\mathrm{JRC} = \mathrm{A}\left(\frac{20}{\mathrm{D}}\right)^{3} \tag{1.1}$$

where *A* is the compliance coefficient in radians/inch-pound.

The importance of correct JRC value of FIJs in modal predictions have been brought out by several researchers (G.M. Henson et al., N. Kumar et al., S.M. Kaplan et al., B. Kumar et al., J.B. Gunda et al., V.L. Alley et al., S.A. Leadbetter et al., C. Roberts et al., 39-52). The JRC is quantified experimentally by static or dynamic method. In static method, one part of the FIJ is mounted on a vertical reaction plate and a crack opening device (COD) is mounted either at top or bottom most location of the joint. Bending moment M is applied at the joint through actuators, joint opening δ is measured from the COD. Based on the measurements of δ and M, the JRC is calculated as $\theta = \delta/D$; JRC= θ/M; where θ is the joint rotation and D is the pitch-circle diameter of the bolts. In dynamic method, JRC is determined in the ground resonance test of the flight vehicle where the first three fundamental frequencies are measured. Now, the FV is modelled numerically based on beam or shell elements with (E_iI_i) variations along the length. FIJs are modelled as rotational springs (k_j) with an approximate JRC, where i = 1 to 6 and j = 1 to 5. Modal analysis is carried out through FEA. The JRC of rotational springs are adjusted *by trial-and-error* until the measured fundamental frequencies and mode shapes match with the FEA predictions.

1.2.2 Research Gaps

There are appreciable research gaps in quantifying JRC of FIJ in a flight vehicle. The significant gaps are as summarized below.

- A theoretical model to predict JRC of FIJ is not available.
- Prediction of JRC is not well matured by numerical methods.
- JRCs are always experimentally determined for a given type of FIJ.
- There is no clarity on number and size of fastener for achieving a required JRC of a FIJ.

1.3 Thesis Objectives

The background, detailed review of literature and the identified research gaps have led to the formulation of the research objective for the thesis. Accordingly, the objectives of the present research are as given below.

1. Comprehensive review of state-of-the art flight intersection joints.
2. Formulate a mechanics based theoretical model applicable for JRC of FIJs.
   a) Develop a simplified numerical and experimental procedure to determine local joint stiffness.
   b) Compute the JRC of full FIJ from theoretical model using above determined local joint stiffness.
3. Establish a numerical simulation procedure to determine JRC of FIJ and compare with theoretical predictions
4. Characterise the FIJ through numerical simulations by studying the effect of a) Pre-tightening; b) Number of studs; c) Size of studs; d) Stud-pocket geometric parameters; e) Increase in diameter of FIJ on JRC and f) Combined bending moment and axial force on FIJ.
5. Design and realise an experimental set-up; experimentally measure *JRC* and validate theoretical and numerical predictions.

1.4 Organization of Thesis

The thesis will focus on modelling and evaluation of tension type FIJ in different chapters. The Chapter-1 will provide a brief background and an introduction to the FIJs, requirements, motivation, research gaps and research objectives. The Chapter-2 focuses on a comprehensive literature review carried out on general engineering joints, bolted circular flange joints in tubular structures, and different types of FIJs, their loadings, design and

qualification, etc. The Chapter-3 will provide formulation of theoretical modeling of FIJ which needs the values of the local joint stiffness in tension and compression from numerical and experimental results. The Chapter-4 will present the numerical method to determine JRC of full FIJs considering the effects of pretightening, size of studs, number of studs, geometric parameters, and variation in diameter. The Chapter-5 will elucidate the experimental setup and the experiments carried out on full FIJs and comparison of JRC determined from theoretical, numerical and experimental methods. The Chapter-6 summarizes with conclusions and future work.

1.5 Summary

Launch vehicles and missiles are made by assembly of several airframe sections integrated using a Flight Intersection Joints (FIJs). These FIJs are characterised by a joint property named Joint Rotation Compliance (JRC). Several researchers have carried out elaborate works in characterisation of joints for general engineering applications, tubular flanged joints and flight vehicles. Extensive literature studies divulge the extraction of JRC predominantly using experimental methods with not much detailed research using numerical and theoretical methods. This research gaps gives the motivation to estimate the JRCs of FIJs using numerical and theoretical methods. The objectives for the estimation of JRCs are covered in detail supported with validation of results. The organisation of chapters based on the research objectives is elucidated.

Chapter-2

Review of Flight Intersection Joints

2.1 Introduction

The launch vehicles and missiles are slender flight vehicles configured structurally by interconnection of several airframe sections as shown in Fig.1.1. The airframe structural geometry is commonly made of cylindrical, ogival or conical. This interconnection between one airframe sections with another adjacent airframe section is achieved through intersection joints. Preferably, the flight intersection joints (FIJ) are conformal to the airframe's outer geometric profile without any external projections which in turn may cause aerodynamic drag. Mostly, the FIJs are temporary joints which can be opened or fastened on need. Only in certain uncommon cases, to meet the manufacturing and integration constraints, the airframe structural sections are made separately and then joined at intersections either permanently by welding or semi-permanently by riveting, Maloney *et al.* [1].

Flight intersection joints experience more challenging requirements when compared to the bolted joints used in other engineering applications as they are exposed to more harsh environments during flight. Besides flight loads, they are also subjected to operational loads due to handling (i.e. lifting during loading and unloading), articulation (i.e. positioning from horizontal to vertical or at an inclination before launch) and transportation (through a launcher or a transporter). Several types of intersection joints are commonly adopted in practice and the selection of a particular type depends upon the available internal volume, geometry, material, size and configuration of the flight airframe sections, and the kind of joint stiffness, which has a vital impact on the global behaviour of the structure that is acceptable to the flight vehicle. The intersection joints are characterised by the joint compliance and the capability to withstand the flight, transportation and handling loads.

Although there are several types of flight intersection joints, their engineering design, constructional details and concepts are different from each other (Maloney *et al.*, Hillmer, Lasker *et al.* and Gharouni *et al.* 1-5). But their loadings and method of prediction of joint stiffness can be closely related to the mechanics of bolted circular flange joints adopted in tubular structures as shown in Fig. 2.1, which are commonly found in general engineering applications. Significant research has been carried out for many years on bolted circular flange joints in tubular structures and different methods for the design of these joints have been

developed. On the other hand, comparatively, the quantum of research on FIJs is very small and only limited knowledge is published in open literature. The design of FIJs relied more on meeting functional and stiffness requirements based on elaborate experiments and limited theoretical studies. But the well-established concepts and the method of analysis of bolted circular flange joints in tubular structures can be extended to develop the theoretical models and numerical analysis of FIJs. Further, considerable research has been carried out on predicting the joint stiffness and clamping force distribution in bolted joints used in general engineering applications. These studies have brought out simplified theoretical models, validated mostly by finite element analyses (FEA) and in few cases by experiments. These studies helped in quantifying the joint stiffness and clamping force distribution in FIJs. Therefore, it is recommended to briefly review the research on 1) bolted circular flange joints in tubular structures, and 2) bolted joints used in general engineering applications before moving on to the detailed review of FIJs.

2.1.1. Bolted circular flange joints in tubular structures

The bolted circular flange joints in tubular structures were investigated initially under the action of axial forces only for many years and subsequently followed by addition of bending moments in the last 40 years.

2.1.1.1 Under action of axial forces only

Until 1985, the design of the bolted circular flange joints in tubular structures relied on few empirical formulations and guidelines generated based on a large number of tests by Rockey and Griffiths [7], and researchers from British Steel Corporation [8]. These formulations and guidelines were subsequently incorporated in few design codes such as British Standards BS8100 [9] for the design of towers and masts, and Stelco design manual [10] for arriving at the flange thickness and stiffness to resist prying action in hollow structural steel connections. Experiments and theoretical analysis on circular flange joints under tensile loads have been carried out by Igarashi *et al.* [11, 12] in Japan based on limit analysis and an approximate model for the determination of flange thickness and number of bolts in a tubular joint has been proposed. Similarly, based on ultimate limit state static resistance of bolted circular flanges governed by the attached tubular section, Kato and Hirose [13] proposed a yield line mechanism which is almost axisymmetric and quite similar to the failure mode proposed by Igarashi *et al.* [11, 12]. These methods have been adopted in the design guide for circular hollow section (CHS) joints by CIDECT13 (Comite International pour le Developpement et

1'Etude de la Construction Tubulaire) [14] and was incorporated in a book by Packer and Henderson [15]. This research helped to determine the thickness of flange and the required total bolt tension capacity which in turn is used to decide the diameter, number and the grade of bolts, for the joint.

Cao and Bell [16-18] conducted detailed theoretical, numerical and experimental studies on bolted circular flange joints. They performed numerical studies through FEA, adopted axisymmetric and 3-D models, and analysed a number of joints with different dimensions and bolt arrangements. They obtained bolt forces, contact forces between flanges, and displacements and stresses in the tubes and the flanges. They investigated the influences of bolt preload, tension force and joint geometry on joint behaviour. Subsequently, they conducted experiments and confirmed the results of FEA. They reported that the total bolt force in a tubular joint may be much higher than 120 percent of the tension force applied to the joint. Cao and Packer [19] proposed models based on the static resistance of flange joints of circular tubes, as shown in Fig. 2.1, under tensile load from an elastic analysis leading to a safer design as compared to the limit analysis of previous researchers that provided an optimal solution. In Fig. 2.1, the D_f is the diameter of flange, D_p is the pitch circle diameter of bolts, d is the bolt diameter, D is the diameter of the tube analogous to the flight airframe diameter and T is the tension on the joint.

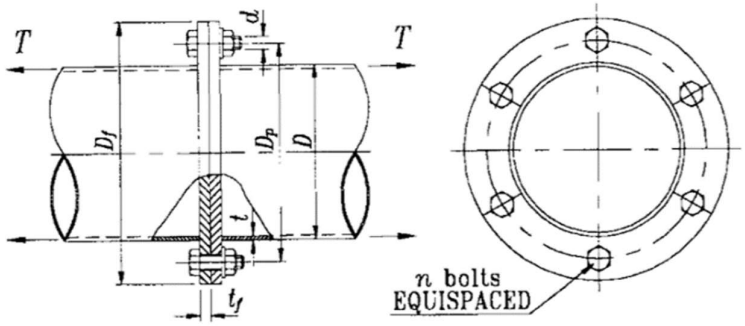

Fig. 2.1. A typical bolted circular flange joint joining two hollow cylindrical (tubular) structures [18]

They [19] proposed new design method with design charts to decide the flange thickness and number of bolts for a tubular joint. The bending moment at the bolt pitch circle is given as

$$M = \frac{T}{8\pi}\left[(1-\nu)\frac{D_f^2-D_p^2}{D_f^2}\left(\mu - \frac{(D-t)^2}{D_p^2}\right) + 2(1+\nu)ln\frac{D_f}{D_p}(\mu-1)\right] \quad (2.1)$$

where v is the Poisson's ratio, μ is the slope of the bolt force T_b versus the tension force T on the joint as shown in Fig. 2.2, T_{bo} is the total bolt preload in the joint and γ is used to take account of bolt preload.

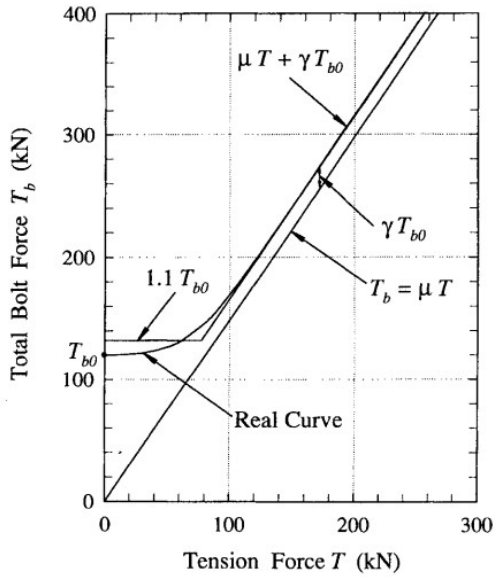

Fig. 2.2. Relationship between bolt force and the tension force in the joint [18]

Close observation on the results [16-19] demonstrate that relatively thin flanges introduces prying action on the joint where the joint is resisted by the tensile limit of the bolts and on the other hand, for the given tensile capacity of the bolts, thicker flanges can reduce prying force and thereby improve the tubular joints' stiffness. Stamatopoulos and Ermpopoulos [20] developed a model based on the limit analysis where all the components of the connection are assumed to reach their full plastic resistance at the ultimate state and excluded the tube wall buckling. Based on the work of Igarashi *et al.* [11, 12], Couchaux et al. [21] derived a closed form solution for the ultimate tensile resistance of a bolted flange joint considering the effects of contact between the two opposite flanges, validated through FEA and published experimental results, and shown its validity for a large range of joints. This model accounts the effect of the position of the prying force and the action of the tube on the joint. But the bending moment between tube and flange is neglected in all the aforementioned models [11-21].

2.1.1.2 Under combined bending moment and axial forces

The models, subsequently proposed by researchers [22-25] included the effect of bending moment along with axial forces on the tubular flanged joints. A mechanical model of

a non-preloaded flanged bolted tubular joint was presented by Kozlowski and Wojnar [23] based on tension and compression components using springs. The stiffness of the springs were defined based on the theoretical and numerical analyses verified by experiments. The position of the neutral axis was calculated based on equilibrium of axial forces in the cross-section. Kozlowski and Wojnar [24] investigated the influence of flange bolted joint's stiffness on the behaviour of steel chimneys under the influence of wind load and vortex shedding. Behaviour of the joint was modelled by springs fixed on bolts' pitch circle diameter. An analytical model using the rule of component method was used. The deformation was obtained using experiments and FEA and introduced into the model. The natural frequency increases when the number of joints increases in the tubular structure. Stiffness of bolted flanged joints in tubular structures can influence the horizontal displacements of the structures, the natural period of the structures and the parameters of vibration damping.

Kozłowski and Wojnar [24] investigated the influence of the stiffness of flange bolted joints on the natural period, critical wind velocity, number of cycles and the horizontal displacements of the steel tubular structures. Behaviour of the joint under combined bending and axial forces was modelled by set of individual springs, fixed on the perimeter of circle i.e. diameter of structural shell of cylinder. The model consists of two types of components i.e. components in the tension zone, characterized by their stiffness k_T and resistance R_T, and the components in the compression zone, characterized by their stiffness k_C and resistance R_C. Couchaux [22] proposed a model to determine the static resistance of a bolted circular flange connection applied for tubular members such as chimneys, pylons of wind turbines, and ski-lift installations, and subjected to combinations of bending moment and axial compressive or tensile loads. This model is based on limit analysis considering two failure modes based on the ductility of tensile part and the shell buckling resistance of compressive part of the bolted connection. For the ductile failure mode, all components reach their plastic resistance, and for the non-ductile failure mode, only the highly stressed component reaches its resistance locally. Azim [26] and Emara *et al.* [27] investigated the bolt tension in a bolted circular flange of a pipe joint subjected to bending moment, using an elasto-plastic material model in FEA and simulated bolts with spring elements. He reported that the bolt tension decreases with the increasing number of bolts and increases with the increase in flange thickness and increasing in pipe diameter. Number of bolts, flange thickness and flange width are the three parameters that influence the bolt tension for a flanged pipe joint.

2.1.2. Bolted joints in general engineering

The prediction of the joint stiffness and clamping force distribution in bolted joints used in general engineering applications is studied. In general engineering, there are three are types of bolted joints according to the methods of loading. They are a) conventional joint, b) axisymmetric loaded joint, and c) eccentrically loaded joint. Few noted research on bolted joints are summarised here. A new approach to load transfer in a bolted joint was proposed by Weissberg *et al.* [28] in which they obtained shear stiffness for a multi row lap joint loaded in tension and represented the joint stiffness as a function of applied load using the experimental load-deflection curve and FEA. Joint characteristic is described by a non-dimensional parameter Z as

$$Z = \left(\frac{t}{d}\right)^3 \frac{E_p}{E_b} \tag{2.2}$$

where Z is the ratio of bending stiffness of the bolt to the plate bearing stiffness and it ranges from 0.2 (rigid bolts) to 2.8 (rigid plates); t is the plate thickness; d is the dimeter of bolt; E_p is the modulus of elasticity of plate; and E_b is the modulus of elasticity of the bolt. Allen [29] determined the joint stiffness of preloaded bolted connections using strain energy calculations i.e. from preload F_i ($=T_{bo}$) versus deflection δ curve as shown in Fig. 2.3. The slope of the curves represents the stiffness of the bolt k_b and members k_m. The areas projected under these curves, represent the stored strain energy in the bolt U_b and members U_m. Knowing the deflections in bolt δ_b and members δ_m, the member and bolt stiffnesses are calculated as

$$k_b = \frac{F_i}{\delta_b} = \frac{F_i^2}{2U_b}; \qquad k_m = \frac{F_i}{\delta_m} = \frac{F_i^2}{2U_m} \tag{2.3}$$

The relation between the strain energy, the stiffness of bolt, and members is defined as

$$\frac{U_b}{U_m} = \frac{k_m}{k_b} \tag{2.4}$$

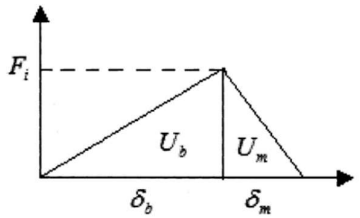

Fig. 2.3. Strain energy driven from force-deflection curve [29]

Zhang and Poirier [30] developed an analytical model for studying the behaviour of axisymmetric loaded bolted joint. Through analytical models, they shown additional member deformations under action of external load, which are the combinations of the a) member compression due to external load, b) member expansion, and c) member thickness dimensional change, seen by the bolt, due to member rotation. Accordingly, they introduced three different

factors such as member rotation stiffness, proportional factor, and varying member stiffness to account them in analytical model. Grosse and Mitchell [31] showed that external loads cause a gradual member separation leading to significantly nonlinear joint stiffness and create significant prying even in an axisymmetric problem. Even a tensile separating force on the joint causes bending effect which has a very significant effect on the bolted joint stiffness. Roy [32] demonstrated that in a bolted joint, a preloaded bolt apply an equal and opposite force to the connected members. The members with the bolt tightened, behave with an equivalent stiffness of the joint, which would always be less than either of the individual stiffnesses. Generally, the bolt will be in tension and members in compression and both are treated as stiff springs exerting the forces in series.

In FEA of bolted joints, many approaches have been adopted to model a bolted joint by different researchers [33-38]. Kim *et al*. [33] represented the bolt by a beam or link element with pretension applied along the axis and positioned through the bolt hole. The ends of these elements are connected to the bolt hole outer edges using rigid links. Sometimes the bolts are modelled as solid elements with externally applied pretension. In modelling the bolted joints in FEA by Montgomery [34], Lehnhoff and Bunyard [35], Wileman and Chowdhuri [36], characteristics like pretension and mating part contact were simulated to understand the joint separation and compression. Pretension was accounted using a pretension element. The solid bolt modelling approach was recommended as the most realistic simulation approach. One of the characteristics that is ignored for the bolting analysis is the effect of threads and friction interaction at the contact surfaces. Rasti [37] compared the joint stiffness of three different types of bolted joints using a detailed FEA. Through FEA, Nassar *et al.* [38] investigated the nonlinear deformation behaviour of clamped bolted joints under a separating service load.

These investigations [28-38], in general engineering bolted joints, helped in quantifying the clamping force distribution through the thickness of the clamped members below the bolt head and nut and also radially along the transverse direction in members. Experimental studies have focused mostly on measuring the force in bolts and also the clamping force just below the bolt head using special types of force sensors. These approaches have been adopted to study the bolted joints used in civil structures, machineries and FIJs.

2.1.3. Flight intersection joints

Traditionally, the knowledge gained in the study of bolted circular flange joints in tubular structures and general engineering bolted joints have been extended to study the

mechanics of FIJs. The prediction of rotational stiffness in these joints have attracted a great interest and few researchers gave a simplified solution considering the bolts as linear springs and their variations of stiffness influenced by the position of springs with respect to neutral axis or the tilting edge [23, 25].

An evaluation of common analysis methods for the bolted joints in launch vehicles was proposed by Henson and Hornish [39]. They showed that the joint stiffness of a FIJ decreases markedly and nonlinearly as soon as an external tensile load is applied; yielding plays no role until the joint is near failure; the initial and immediate softening is due to contact nonlinearity, as the angle surfaces separate; and a large decrease in stiffness under less load can significantly influence the dynamic response of the FIJ. Kumar *et al.* [40] studied the FIJ between aft end of the rocket motor and its nozzle circular flange using a three-dimensional FEA. The approach followed in [26-27, 34] have been extended for this FIJ. The joint is made of stud and nut type where several studs having external threads project at the aft flange of the rocket motor, receives the fore end flange of nozzle and pre-tightened with nuts. This joint meet two important functions viz. a) maintain the structural integrity of the joint itself, and b) prevent the leakage of propulsion gases through the gasket preloaded by bolts. The gas pressure tends to reduce the bolt preload, reduces the gasket compression and tends to separate the flange faces in the FIJ. The flange opening causes bending in the bolts. It is shown that due to the existence of preload, internal gas pressure and bending moment from flight structure, the bolt behaviour is nonlinear which cannot not be easily evaluated by theoretical models and adoption of 3D FEA could provide accurate results matching with experiments.

Kaplan [41] has determined the flexibility coefficients i.e. a measure of joint rotational stiffness for flight structural joint assemblies and reported the challenges in experimental and theoretical determination of the flexibility coefficients and the importance of these values in flight dynamics. Kumar *et al.* [42] and Gunda and Krishna [43] conducted ground resonance test and found the modal frequencies and first three mode shapes of a multi-stage launch vehicle. They also predicted the free vibration response of the launch vehicles through FEA using beam elements representing the airframes and rotational spring elements representing FIJs. They observed significant discrepancies in the predictions as compared to the experimental data. After elaborate investigations, they reported that the value of joint rotational stiffness adopted for the FIJs adversely affected the modal predictions and stressed upon the need for an accurate quantification of joint flexibility or the stiffness of the FIJs. After updating the FEA model with correct joint stiffness for the rotational spring elements, their predictions agreed very well with experiments.

Alley and Gerringer [44] and Leadbetter *et al.* [45] investigated the prediction and measurement of natural vibrations on multi stage launch vehicles where they conducted experimental measurements of free vibration response of launch vehicles and observed considerable difference with the predicted vibration responses. They reported that invariably, computed mode data on launch vehicles which disregard local influences at FIJs will result in frequencies higher than actual; therefore, any reasonable approximation to stiffness of FIJ will move the computed results close to reality. Nevertheless, the possibility of assuming joint factors unreasonably large does exist, and consequently such efforts may result in greater errors than would be experienced if totally ignored. Therefore, Alley and Leadbetter [46] provided a guide to joint evaluation which should provide a simple means for approximating the joint rotation constants in a typical launch vehicle through an empirical relation. This can be used for quantifying joint rotational stiffness which can be adopted for theoretical or numerical predictions of free vibration response of the complete flight vehicle.

Due to the classified nature of work, only limited research publications on flight intersection joints are available in open literature. But significant research have been carried out on flight intersection joints, several types of joints have been devised and adopted in practice at various research institutes across the globe. Based on scholar's and supervisors' experience and review of open literature, this chapter, for the first time, attempts to bring out a comprehensive review of flight intersection joints. This review focusses on the classification of FIJs, different loads acting on the flight vehicle and on the FIJ, and prediction and measurements of joint rotational stiffness (JRS).

2.2. Classification of Flight Intersection Joints

The flight intersection joints are broadly classified based on three important parameters such as 1) construction / design, 2) compliance, and 3) fineness.

2.2.1 Based on construction or design

There are several types of flight intersection joints based on their construction and (or) design. All these FIJs can be again classified into two types [1]: 1) non-separable joint, and 2) separable joint, as shown in Figs 2.4 and 2.5, respectively. Non-separable joints are designed for permanent attachment of airframe sections. These non-separable joints are used only in special circumstances and are uncommon. The permanent attachment of two airframe sections

is generally adopted for easiness in manufacturing of individual flight airframes which are subsequently joined together permanently by welding, riveting or bonding. They tend to be stiffer, stronger, consistent and more predictable in their properties by virtue of being a) welded, b) bonded and (or) c) riveted with many rivets. On the other hand, separable joints are more common and primarily designed for ease of assembly and disassembly of any two adjacent airframe sections under field and depot conditions. They are subjected to different static and dynamic loading during service. Pre-tightening torque values are specified for intersection joint fasteners in an attempt to control the interface preloads and to increase the joint rotational stiffness. There are several types of FIJs as shown in Fig. 2.5 [1- 5]. They are a) shear/radial joint, b) threaded coupling ring joint, c) Marman band joint, d) widget ring or Ortman joint, e) field joint, f) tension or stud-pocket joint, and g) special joint with quarter turn bolt.

Shear or radial joint, shown in Fig. 2.5(a), is adopted in three circumstances i.e. 1) when the thickness of the airframe shell bulkhead is smaller such that the radial thickness of the joint is less than about 5 mm, 2) when the load on the fore end airframe section ahead of the joint is less, and 3) when the permissible axial-length of the joint is less than 2*d*-3*d* where *d* is nominal diameter of intersection joint fastener. This is popular in flights with diameter less than 300 mm. Although it provides relatively less joint stiffness by material and geometry but due to its application in reduced or less loadings, this joint qualifies under moderate class of joint. *Threaded coupling ring joint*, shown in Fig. 2.5(b), is a good class of joint but used only for smaller diameter flights because aligning two airframe sections with end threads and joining them with an internally threaded cylindrical nut or a coupler is a challenge for large diameter flights. Further, this joint introduces external circumferential gaps which act as discontinuity in airflow path causing localised drag, kinetic heating and stress concertation. *Marman band joint*, shown in Fig. 2.5(c), is typically a simple joint which takes relatively short duration for joining two airframe sections. A metallic band with a specified internal receiving contour (say trapezoid) is placed over two end bulkheads featured with a projecting external contour. The band is tightened to join the two airframe sections. This can be used in flights irrespective of its diameter but the joint stiffness achievable is moderate to good depending upon the number of Marman bands adopted. It occupies more axial length of about 8*d*-10*d*.

Ortman or Widget ring joint, shown in Fig. 2.5(d) consists of two bulkhead rings assembled from outside through a rectangular hole in the outer cylinder formed due to the ring groove present on both the fore and aft airframe sections. This kind of joint is used for smaller diameter airframes up to 600 mm whenever there is a constraint of minimal mass for the FIJ. This type of joint takes considerable time for integration of two adjacent airframe section and

needs special tools. The joint stiffness achievable is moderate and it occupies an axial length of about 5*d*-10*d*. *Field joint*, shown in Fig. 2.5(e), consists of a tang at the rear end of one airframe section and a clevis at the front end of the next immediate airframe section. The two airframe sections are assembled and aligned to match the radial pin holes in both the airframe sections and integrated with number of radial pins which are externally protected with circumferential pin retainers. This type of joints are used for airframes of large diameter with stringent pressure requirements. This is more commonly adopted for joining rocket motor end with nozzle / base shroud [6]. Integration of this joint takes more duration and it falls under an excellent class of joint based on its joint stiffness.

Tension or stud-pocket type of intersection joint, shown in Fig. 2.5(f), is featured with threaded studs protruding from end bulkhead of one airframe section which can enter in to the receiving holes in the front end bulkhead of adjacent airframe section. These holes will lead into pockets where nuts can be inserted and tightened with the studs. This is conformal with airframe profile and provides good to excellent class of joint with relatively high intersection joint rotational stiffness (JRS) depending upon the number of studs adopted. But aligning two airframe sections, inserting the studs in respective holes in other bulkhead, tightening and torqueing the nuts take considerable time. This joint is most common but needs about 3*d*-4*d* for radial thickness of airframe shell and 6*d*-8*d* for axial length. *Special joint with quarter turn bolt*, as shown in Fig. 2.5(g), is featured with a bolt hinged at its bottom to one end of bulkhead in an airframe section which can be rotated through quarter turn and inserted radially on the slot in the adjacent bulkhead in another airframe section and tightened with a nut. Number of such quarter turn bolts will be used. Minimum will be 6 and maximum number of bolts can range from 12 to 48 or more depending upon the diameter of the flight airframe and the loads acting on the joint. This type of intersection joint takes relatively less duration for integration of two airframe sections. This FIJ retains the advantages of good to excellent joint stiffness as offered by a stud-pocket class of an intersection joint. The relative characteristics of different types of separable flight intersection joints are summarised and provided in Table 2.1.

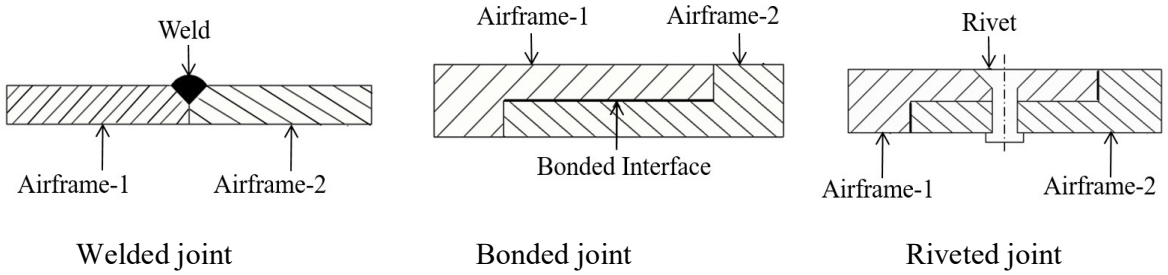

Fig. 2.4. Non-separable flight intersection joints [1]

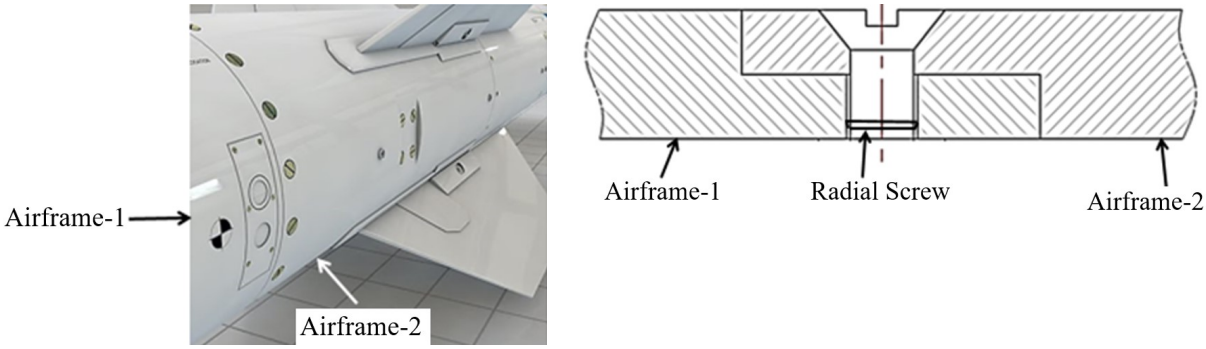

a) Shear / radial flight intersection joint [1]

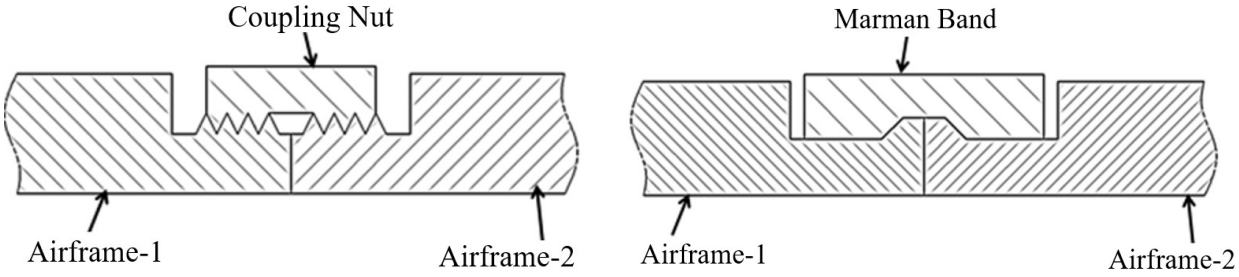

b) Threaded coupling ring intersection joint [3]

c) Merman band intersection joint [3]

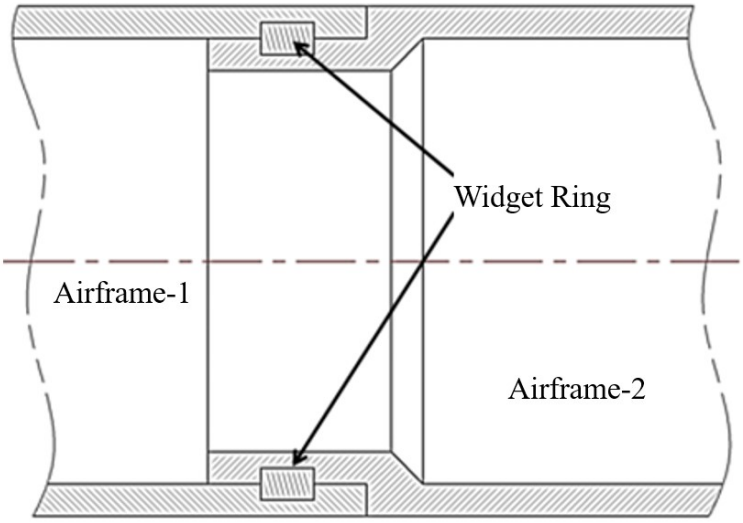

d) Widget ring or Ortman intersection joint [4]

e) Field or land type of FIJ [6]

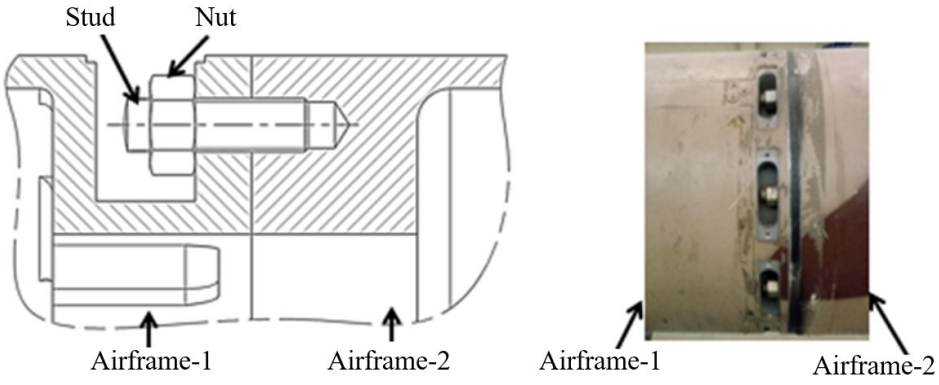

f) Tension joint or stud-pocket type of FIJ

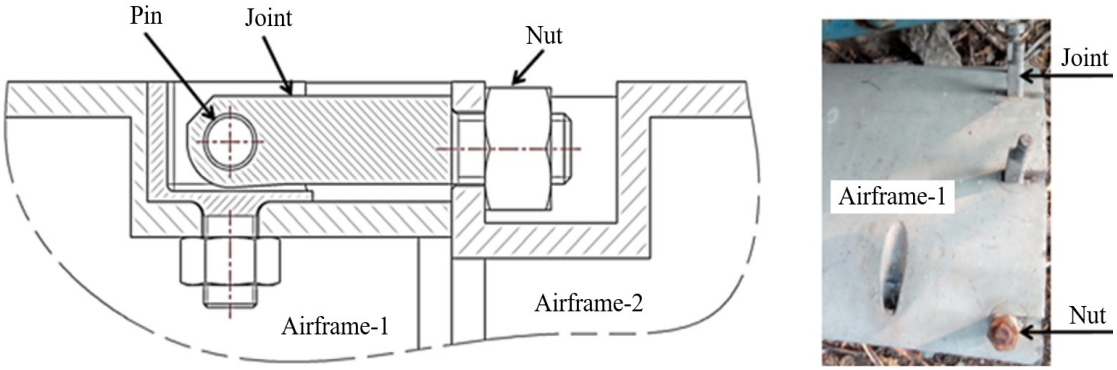

g) Special joint with a quarter-turn bolt

Fig. 2.5. Different types of separable flight intersection joints

Table 2.1. Characteristics of different types of separable flight intersection joints

S. No.	Type of FIJ	Minimum radial thickness of joint	Minimum axial length of joint	Relative joint stiffness	Easiness in integration and time taken	Airframe Profile Continuity	Airframe Diameter Range
1	Shear or radial	1.5d – 2d	2d – 2.5d	Moderate	Easy; moderate	Ensured	< 300 mm.
2	Threaded	10 mm – 30 mm	30 mm – 100 mm	Good	Easy; moderate	Two external discontinuities	300 mm to 500 mm
3	Marman band	3d – 4d	5d – 10d	Moderate to Good	Very easy; less	Ensured	Any diameter
4	Widget ring or Ortman	3d – 4d	5d –10d	Moderate to Good	Easy; moderate	Ensured	300 mm to 600 mm
5	Field or land	1.5d – 2d	5d – 10d	Excellent	Difficult; more	Ensured	> 600 mm
6	Tension or stud-pocket	3d – 4d	6d – 8d	Good to Excellent	Difficult; more	Ensured; Pockets can be closed	> 300 mm
7	Special type with quarter turn bolt	3d – 4d	6d –8d	Good to Excellent	Moderate; moderate	Intermittent discontinuities but can closed	> 300 mm

2.2.2 Based on joint compliance

The flight intersection joints are classified based on the joint compliance that characterises whether the joint has adequate rotational and axial stiffness or not [45]. The requirement for airframe's stiffness comes from various system requirements like static and dynamic structural loads, aero elasticity margins, aero elastic coupling with guidance and control, structural dynamic loads, logistic/transportation, and flight environment. Based on joint compliance i.e. joint rotational compliance (JRC) which is nothing but a representation of joint flexibility or the inverse of joint stiffness, the flight intersection joints can be classified as a) loose, b) moderate, c) good, and d) excellent [43] as shown in Fig. 2.6 and examples shown in Table 2.2. An interface joint constitutes an effective load path which results in significant reduction in effective stiffness at the joint interface and its vicinity. Joint compliance effects typically account for more than 30% of the total elastic deformation of a flight in its primary bending modes. Therefore, it is very important to accurately estimate the intersection joint compliances.

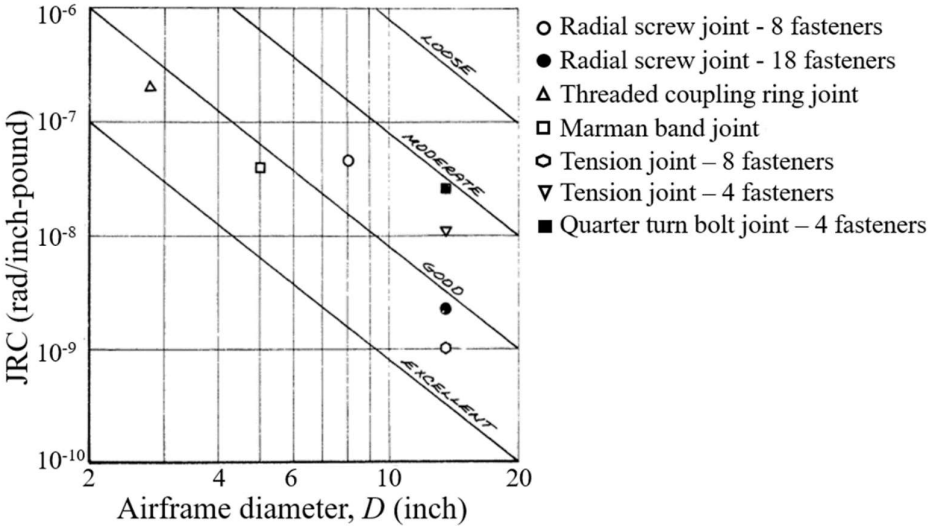

Fig. 2.6. Classification of FIJ based on JRC [44]

Table 2.2. Compliance based classification of FIJ with examples [46]

S. No.	Compliance based classification of FIJ	Joint description	Illustrative example
1	Excellent	Butt welded, heavy bolted and preloaded	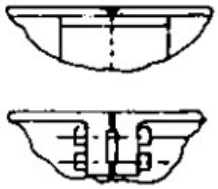
2	Good	Heavy flange bolted, threaded, Marman band joint, etc.	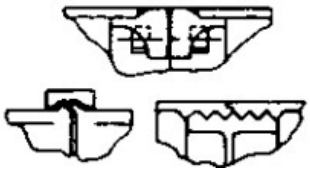
3	Moderate	Riveted, lap riveted to inner ring screw section without butt, widget type or land type	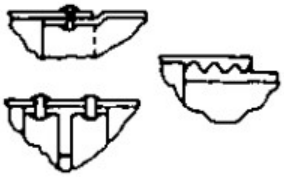
4	Loose	Light flanges, bolted or riveted lapped with screw fasteners equally spaced brackets; non pre-tightened joint	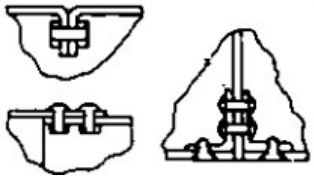

2.2.3 Based on fineness of flight vehicle

Fineness is the ratio of flight vehicle's length to the diameter [5]. This is also called as the slenderness ratio of flight. Small fineness flight vehicles use radial or threaded joints, medium fineness flight vehicles use radial or stud-pocket joints and high fineness flight vehicles use stud-pocket or special joints to meet the desired joint stiffness requirements.

2.3. Loads on Flight Intersection Joints

The flight vehicle body experiences different kinds of loads during flight, launch, handling, transportation, and storage conditions which are directly transmitted to the flight intersection joints that interconnects different airframe sections in the flight vehicle.

2.3.1 Flight loads

2.3.1.1 External forces and internal loads

The flight loads are experienced by the intersection joints due to structural loads on the flight vehicle generated from rocket thrust, aerodynamic drag and lift, and inertial forces. These structural loads are computed considering all possible flight trajectories. These flight loads can be converted as bending moments, and shear and axial forces as shown in Fig. 2.7(a) which can be directly adopted for design and analysis of flight airframe sections and flight intersection joints. The type of intersection joint influences the joint rotational stiffness and strength that can take care of these flight loads.

The highest aerodynamic loads experienced by the vehicle's airframe occur at maximum dynamic pressure q. Typically, the higher air (or vehicle's) velocity gives highest q at a given altitude which generally occurs just at propulsion burnout. If the vehicle is hit by a strong side-gust at maximum q, then the aerodynamic loads caused by the gust can cause structural breakup of the vehicle, if the vehicle is not designed for these aerodynamic loads. Yet another type of loading apart from the wind pressure is the aerodynamic pressure acting normal to the airframe skin. If this external pressure is greater than the compartment's internal pressure, then all the strengthening benefits of a pressurised skin are nullified, and the stringers simply behave as beam columns, which must be stabilised against collapse by increasing their thickness, Newlands *et al.* [47]. Apart from wind, both thrust and aerodynamic loads which are treated mathematically as forces externally applied to the vehicle, vary in magnitude and direction, and are resisted only by the vehicles' inertia. This inertial resistance causes inertial loads within the structure as it accelerates in response to the external forces. The distribution of the aerodynamic forces (normal and axial) along the flight vehicle determines how the vehicle suffers when gusts or wind shears (i.e. rate of change of wind velocity with altitude) cause sudden angles of attack α.

A more typical flight vehicle loading is shown in Fig. 2.7(a) where the vehicle is accelerating upwards due to the nose and fin lift, but it would also be rotating about its centre of gravity (CG). The resulting inertial loads from engine mass M_e and avionics mass M_a are supported equally by fore and aft bulkheads, and the main payload gives a distributed load along the fuselage wall. Maximum shear forces and therefore the worst bending moments will often occur at the instant of maximum $q\alpha$. This is where the aerodynamic loads are maximum, and

the lateral and rotational accelerations are also maximum (maximum vehicle response), giving the highest inertial loads.

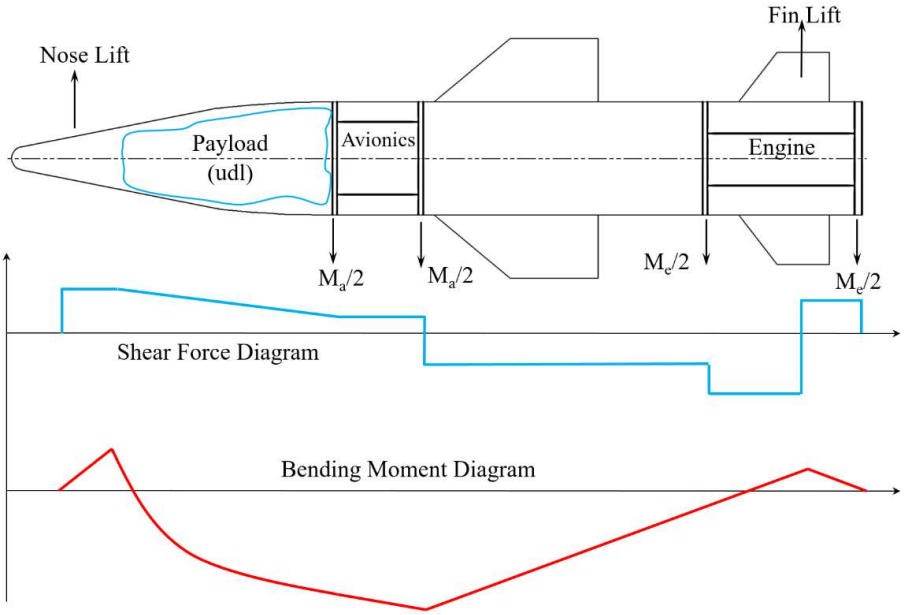

(a) Typical shear force and bending moment on a flight vehicle

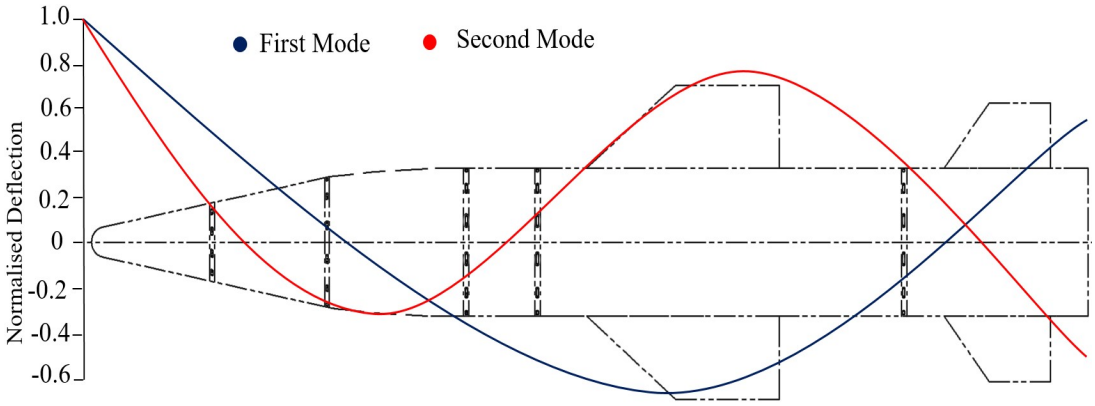

(b) Flexural modes on a slender flight vehicle

Fig. 2.7. Typical flight loads on a flight vehicle influencing the design of FIJ

2.3.1.2 Natural flexural modes

The flight vehicle acts as a rigid body, bends out of shape slightly in response to the various loadings. As the fuselage is free at both ends (unrestrained), the forces and masses along the fuselage cause the elastic bending to acquire a definite, predictable shape or natural mode,

but the shape is time-dependant i.e. the fuselage will bend in and out of shape at a set frequency. It is a combination of several independent natural modes: each mode vibrates at a certain (successively higher) frequency which may or may not be set in motion by gusts and turbulence of a similar frequency. These bending modes have particular shapes as shown in Fig. 2.7(b). It is worth noting that successively higher bending modes have less and less effect (smaller amplitudes), so they can be neglected. Typically, when analysing a large launch vehicle, attention is paid to only the first three bending modes.

The slender flight vehicle can be modelled as a simple one-dimensional beam with length along the fuselage only. It has been observed and reported that the required number of fuselage mass stations should be approximately 10 times the number corresponding to the highest elastic bending mode to be calculated. For example, if three elastic bending modes are to be calculated, then approximately 30 mass stations are required to represent adequately the bending dynamics of the third mode. The prediction of elastic modes require intersection joints' rotational stiffness. The determination of elastic modes and Eigen values of flight vehicle are essential to design flight structure to withstand aero-elasticity and prevent flutter phenomena, Maloney *et al.* [1, 3]. Besides above loads, all flight intersection joints are subjected to random and harmonic vibrations during flight and thermal loads due to kinetic heating. There shall be acceptable or no relaxation in joint stiffness under these loads.

2.3.2 Launch loads

Launch loads can be classified under two types such as 1) after articulation and before launch, and 2) during launch.

2.3.2.1. After articulation and before launch

The flight vehicles are articulated from horizontal to vertical direction or at an inclination. Generally, they are launched in vertical direction except in very few special cases where they are launched at an angle. After reaching the launch orientation and before launch as shown in Fig. 2.8, the flight vehicle is subjected to bending moments due to wind loads acting at the center of pressure of the flight vehicle. The flight intersection joints resist the wind induced bending moments and also experience the axial compressive force due to self-weight of the vehicle ahead of the intersection joint. The maximum bending moment is actually resisted by certain type of a hold-release structural or mechanical arrangement featured at the aft end of the flight vehicle.

2.3.2.2. During launch

During launch, the flight vehicle is a free body and subjected to different forces and moments as shown in Fig. 2.9. They are a) bending moment due to wind load F_w acting at centre of pressure *CP* of the vehicle which is at a distance x_p from the nose-tip, b) axial compressive downward force due to aerodynamic drag F_d acting along the geometric centre of the body, c) self-weight *W* of the launch vehicle acting through its centre of gravity *CG*, d) moment due to *W* passing through the lateral CG offset *a*, e) axial upward thrust force *T* transmitted from the rocket motor along the longitudinal axis of the vehicle, and f) the bending moment generated on the vehicle due to F_s, the side force generated due to the thrust axis misalignment, if any, with the longitudinal axis of the vehicle. All these loads are resisted by the FIJs.

Fig. 2.8. After articulation and before launch [48]

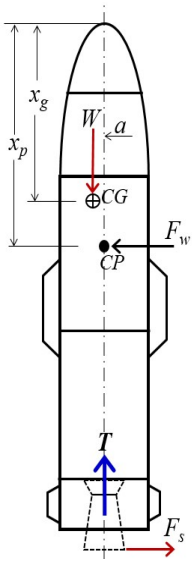

Fig. 2.9. Different forces during launch

2.3.3 Transportation loads

The flight vehicle is transported to launch site through a carrier vehicle or a launcher as shown in Fig. 2.10. The flight vehicle is supported at any two bulkhead locations in the airframe along the length such that the longitudinal location of centre of gravity lies in between the selected two bulkhead supports. During this transportation, the flight vehicle is subjected to a) longitudinal accelerations or retardations transmitted from the carrier vehicle, b) lateral accelerations due to centripetal force while negotiating a curve, and c) vertical accelerations

due to road irregularities. These loads cause bending moments and shear forces on the flight vehicle which are in turn resisted by FIJs and airframe shell.

Fig. 2.10. Carrier vehicle cum launcher [49]

2.3.4 Handling loads

The flight vehicles are generally handled i.e. lifted at ground or hangar using a lifting beam with wire ropes or belts or lifting lugs connecting the flight vehicle at two stations on either side of the longitudinal location of centre of gravity as shown in Fig. 2.11. This lifting condition simulates the flight vehicle as a beam transversely loaded with a distributed load due to the self-weight of the vehicle and support reactions at two hooking points. This condition also introduces bending moments and shear forces which are resisted by the FIJs.

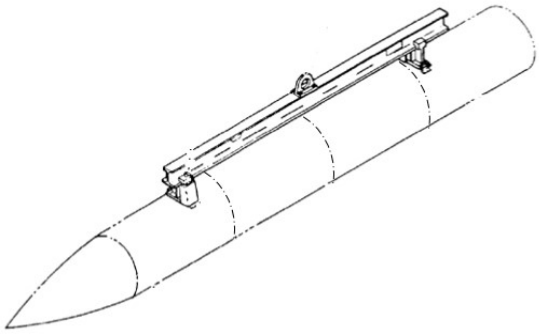

Fig. 2.11. Lifting of flight vehicles [50]

2.3.5 Storage loads

Even during storage, the flight vehicle is under the influence of bending moment and shear forces caused by the self-weight and the support reactions. The prolonged years of storage under same loading condition introduces creep load on flight intersection joints. These loads are withstood by the stiffness of the flight intersection joints. There is a possibility of certain amount of joint relaxation due to creep and thereby reduction in joint stiffness.

2.4. Joint Rotational Stiffness

A flight intersection joint is characterised by the value of its joint rotational stiffness (JRS) which is nothing but the resistance offered by the intersection joint against unit rotation under an externally applied bending moment, expressed in Nm/rad. It is also equally represented in terms of joint rotational compliance (JRC) expressed in rad/Nm, Alley and Leadbetter [46]. JRC is a direct measure of the rotational flexibility offered by the joint under an externally applied unit bending moment and it is the inverse of JRS. An excellent joint should exhibit a very high value of JRS and a very low value of JRC. A high value of JRS ensures that the FIJ acts as a near-rigid connection between two airframe sections and thereby exhibiting a continuity in natural mode shape when excited by any external disturbances like aerodynamics or any internal stimuli like the vibration or the force transmitted by an internal on-board system. Higher value of JRS and subsequent modal continuity help in improving the resistance offered by the flight structure in sustaining the interaction between control-structure-aerodynamics. There are few predictive and experimental methods for quantifying the JRS.

2.4.1. Predictive methods for JRS

There are few predictive methods based on theoretical and empirical approaches for quantifying the JRS based on suitable approximations [23, 25, and 46]. However, for any new flight, it is measured and quantified through an experimental setup.

2.4.1.1. Empirical method for JRS

In many launch vehicles, significant local contributions to flexure originate at FIJs and that these joint effects must be included in analyses involving flexure, e.g. natural vibration. Contributions of the joints to the deflections generally defy rigorous analytical description. Such contributions are consistently encountered from looseness in screwed joints, thread deflections, flange flexibility, plate and shell deformations that are not within the confines of beam theory, Alley and Gerringer [44] and Leadbetter *et al.* [45]. Since, it is generally impractical to evaluate these effects analytically, the problem has been treated empirically at NASA Langley Research Center with satisfactory results in quantification of JRC which is used in the determination of natural vibration and aero elastic characteristics [44-46].

One approach in estimating the joint compliance was proposed empirically by Alley and Leadbetter [45]. This is used widely and derived from launch vehicles' test data. This gives the relationship between the joint flexural compliance *C*, airframe diameter *D* at the joint location and the joint classification as

$$C = A\left(\frac{20}{D}\right)^3 \tag{2.5}$$

where *C* is nothing but the JRC in radians/inch-pound, *D* is in inch, and *A* is the compliance coefficient in radians/inch-pound. They [46] also established a set of curves as shown in Fig. 2.12, relating JRC with airframe shell diameter based on 10 measured values of joint compliance for a variety of different classes of joints. Because of the limited quantity of measured data, the curves that show the variation in JRC with diameter were not only empirically established but were also based on the assumption that JRC is inversely proportional to the third power of the diameter. This is in accordance with the theoretical variation in flexibility of geometrically similar joints, and the resulting curves proved to be in good agreement with the measured data.

The magnitude of compliance coefficient A is a function of compliance classification as given in Table 3. They have conducted nine experiments with different flight diameters, subjected to externally applied bending moment, measured JRC and classified the FIJs based on the value of JRC as provided in Table 2.3 and Fig. 2.12. The classification of FIJ has four ratings such as excellent, good, moderate and loose as mentioned previously. The stiffness rating is the NASA's rating that suggested factors of ten increase in compliance progressing from each level-excellent, good, moderate, and loose. Thus a moderate joint would be 10 times as compliant as a good joint and 100 times as compliant as an excellent joint.

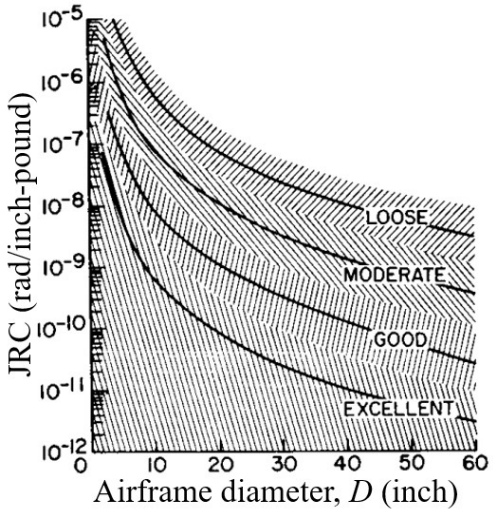

Fig. 2.12. Joint classification based on JRC for different airframe diameters [46]

Table 2.3. Compliance classification for FIJs [44]

S. No.	Compliance classification	Compliance coefficient- A			
		Nominal		Range	
		(rad/Nm)	(rad/inch-pound)	(rad/Nm)	(rad/inch-pound)
1	Excellent	8.851×10^{-10}	$1(10)^{-10}$	$< 26.553 \times 10^{-10}$	$< 3(10)^{-10}$
2	Good	8.851×10^{-9}	$1(10)^{-9}$	26.553×10^{-10} to 26.553×10^{-9}	$3(10)^{-10}$ to $3(10)^{-9}$
3	Moderate	8.851×10^{-8}	$1(10)^{-8}$	26.553×10^{-9} to 26.553×10^{-8}	$3(10)^{-9}$ to $3(10)^{-8}$
4	Loose	8.851×10^{-7}	$1(10)^{-7}$	$> 26.553 \times 10^{-8}$	$> 3(10)^{-8}$

2.4.1.2 Theoretical method for JRS

Few researchers proposed approximate theoretical methods for the determination of JRS. These methods were evolved considering 1) the bolts as elastic springs, and 2) kinematics of joint rotation centred about the bottom most pivot point in the joint. Mostly they were developed for bolted circular flanged joints connecting two cylindrical tubes as explained in Sec-2.1.1. Kozłowski and Wojnar [23] proposed a mechanical model to compute the initial JRS of such a flanged bolted joint under the combined action of separating bending moment *M* and axial force *N*. Further, Couchaux *et al.* [22] also introduced a similar mechanical model for

prediction of JRS with only difference being the theoretical determination of stiffnesses without resorting to experiments and numerical simulations. Although these methods have been developed for flanged bolted joints in cylindrical tubes, these approaches are very well applicable to FIJs and can be adopted in practice for calculation of JRS in flight intersection joints.

2.4.2. Experimental method for JRS

The computation of JRS of a FIJ based on theoretical or empirical methods described above is quite cumbersome and provides only an approximate measure. Therefore, the popular method of determination of JRS is by experiments. There are two methods in experimental measurement of JRS namely direct (or static) and indirect (or dynamic) method as described here.

2.4.2.1 Direct method

The direct method is a static method. In this experimental approach, one part of the FIJ is mounted on a vertical reaction plate and a crack opening device is mounted either at top or bottom most location at the joint intersection plane, depending upon whether the applied bending moment is sagging or hogging. The external bending moment M is applied at the other part of the joint through actuators at extended rigid connections as shown in Fig. 2.13. The opening of the joint δ is measured using a crack opening device for every stage of the applied moment. This moment is applied until 200% of the maximum service bending moment. This service bending moment is generally limited to 20% of the moment corresponding to the first yield moment of the airframe section material. Based on the measurements of δ and M, the JRS is calculated as

$$\theta = \frac{\delta}{D} \tag{2.6}$$

$$JRS = \frac{M}{\theta} \tag{2.7}$$

where θ is the joint rotation and D is the pitch-circle diameter of the bolts.

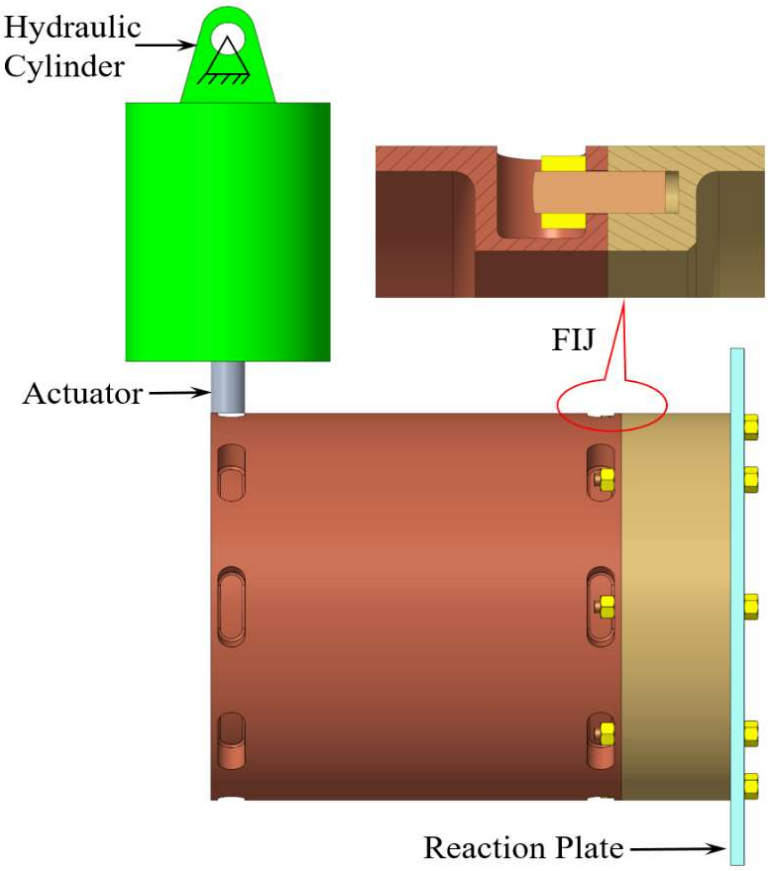

Fig. 2.13. Experimental setup for JRS measurement

2.4.2.2 Indirect method

Indirect method is another common experimental based technique where attempt is to match, by trial and error, a measured set of natural vibration mode shapes and frequencies of the flight vehicle, assuming joint compliances to be the only unknowns in the model analysis representation. The indirect method is a dynamical method where the JRS of the FIJ is determined indirectly through a ground resonance test of the fully integrated flight vehicle followed by numerical simulations. All airframe sections of the flight are integrated to achieve the specified mass properties based on mission requirement such as mass, location of centre of gravity along three principal coordinate axes and mass moments of inertia about three axes. The integrated flight vehicle is subjected to a modal test (i.e. a ground resonance test) as shown in Fig. 2.14 and first three fundamental frequencies and mode shapes are measured.

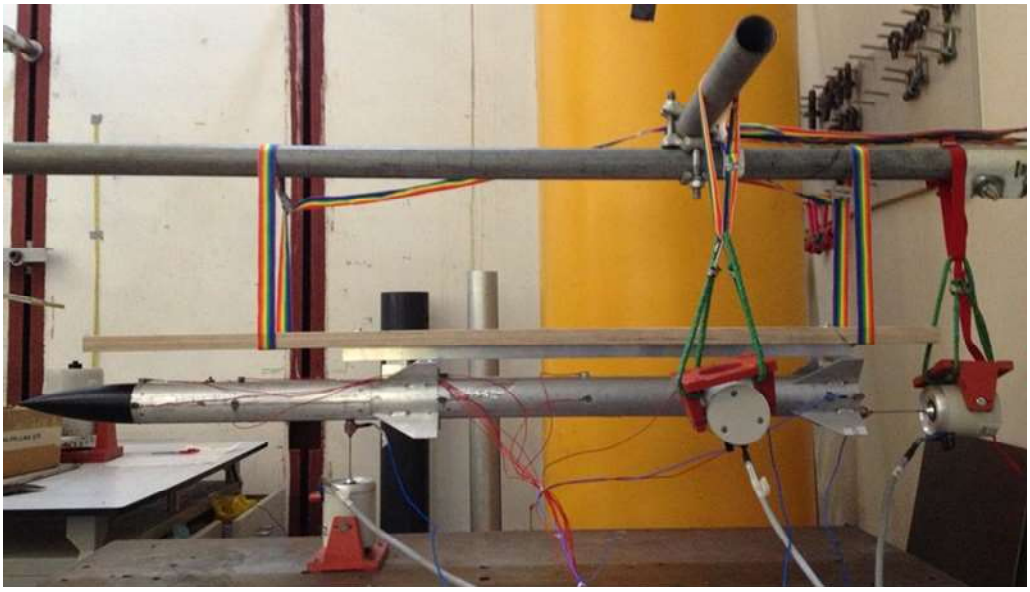

Fig. 2.14. Ground resonance test of a fully integrated flight vehicle [51]

Now, the full flight vehicle is modelled in finite element method, based on beam or shell elements with appropriate flexural rigidity (E_iI_i) variations along the length. The FIJs are initially modelled as rotational springs (k_i) with an approximate JRS as shown in Fig. 2.15, where i = 1 to 6 for EI and i = 1 to 5 for k. Modal analysis is carried out through FEA. The value of JRS in rotational springs are adjusted by trial and error method iteratively until the measured fundamental frequencies and mode shapes are matched with that predicted from FEA.

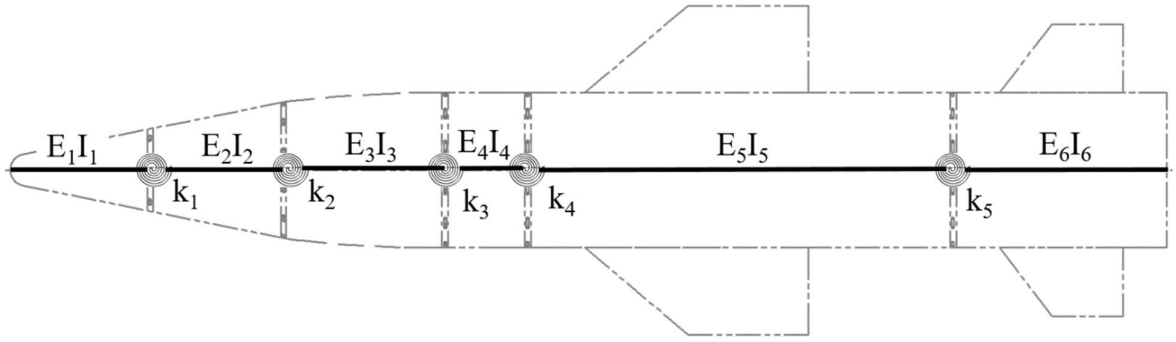

Fig. 2.15. Geometric model of a flight vehicle with rotational springs at FIJs for modal analysis

Alternatively, the fundamental frequency of a flight vehicle can be calculated theoretically. A FIJ constitutes as disturbance in load path which can result in substantial losses in effective stiffness in the vicinity of the joint. The consequences of the joint stiffness losses

will affect the bending modes of the launch vehicle. The bending modes for the airframe are computed using a conventional lumped parameter beam representation in a modified Holzer-Myklestad modal analysis method using numerical codes similar to [3, 5, and 52]. Values for the joint compliances were derived by a trial and error matching of airframe modes measured in ground vibration test. Hence, accurate estimates of joint compliance i.e. JRC is of critical importance in predicting the flight vehicle's dynamic response characteristics.

2.5. Summary

Flight intersection joints play an important role in ensuring the structural integrity of the full flight vehicle. The flight vehicle is an assemblage of individual airframe sections joined at the section's end bulkheads. This chapter provided a detailed discussion on the importance of flight intersection joints, and for the first time, provided a comprehensive review of different types of flight intersection joints, joint characteristics, loads experienced by the joint, and different methods adopted in determination of joint rotational stiffness. Stud-pocket type of intersection joints are common for flights with diameter more than 300 mm and a radial joint is common for flights with less than 300 mm diameter. Although an excellent joint is a preferred choice, achieving it for a separable flight intersection joint is extremely challenging. So the designers aim to at least provide a good class of an intersection joint. Determination of joint stiffness by direct experimental method is a straight forward technique and thus commonly adopted in practice. However, the experimental methods are costly and demand the availability of hardware, thus impeding the apriori quantification of JRC. Adopting empirical or theoretical methods and FEA tools will facilitate in close prediction of JRC and accordingly a suitable FIJ can be selected for a launch vehicle.

Chapter - 3

Theoretical Modeling of JRC of a Tension Type FIJ

3.1. Introduction

The joint rotational compliance (JRC) of a flight intersection joint (FIJ) is an important parameter in the structural design and analysis of a launch vehicle. The JRC is always quantified through extensive experiments due to non-availability of a reliable theoretical or numerical model. The design of FIJs, so far, has relied more on meeting functional and stiffness requirements based on elaborate experiments supported with limited theoretical and analytical studies.

Theoretical or reliable numerical methods to quantify the JRC of a FIJ is not available in literature. This parameter is always experimentally determined through elaborate experimental setup. However, by careful observation, one can understand its close similarity with bolted circular flange joints in tubular structures used in general engineering applications. However, the bolted circular flange joints in tubular structures are not externally conformal to the outer diameter of the tube and therefore, cannot be adopted as FIJ. The underlying concepts adopted in determining the joint stiffness of these bolted circular flange joints can lay a foundation for developing a theoretical model for the FIJ.

This chapter attempts to bring out an analytical model for determining the JRC of a tension type i.e. stud-pocket type FIJ. This is formulated based on the mechanics of bolted circular flanged joints which in turn depends on modelling of localised component joint stiffness. The local component joint stiffness is modelled and quantified through numerical methods, and verified through experiments.

3.2. Theoretical model for the flight intersection joint

A typical tension type FIJ has a stud-pocket type flight intersection joint consists of studs on the front bulkhead of the airframe Section-II. The rear bulkhead of the airframe Section-I consists of pockets with holes for the entry of studs from the front end of the airframe Section-II. The airframe sections are joined together using washers and nuts. These studs and respective pockets are equi-spaced on the airframe section on a particular pitch circle diameter. An exploded view of a FIJ is shown in Fig. 3.1.

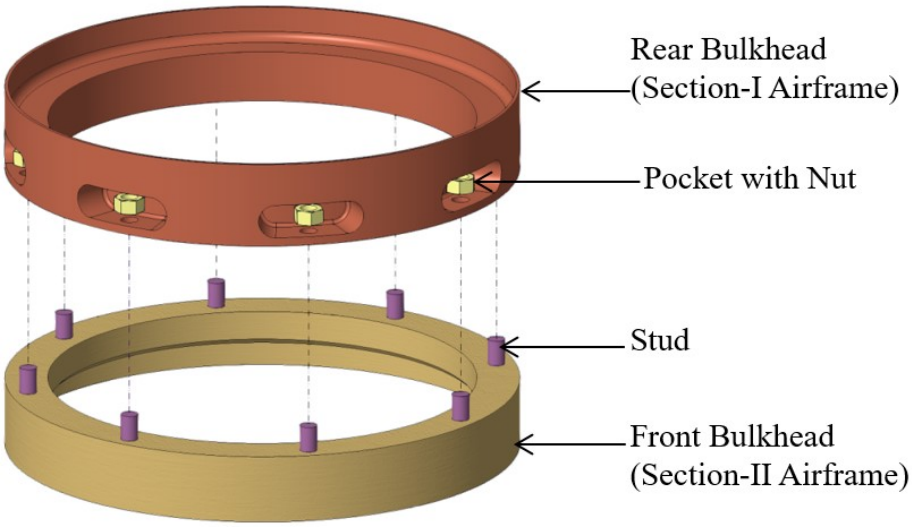

Fig. 3.1. Exploded view of a stud-pocket type of flight intersection joint

The FIJs are subjected to axial forces and bending moments during its flight under the influence of aerodynamic, inertial and elastic loads. The FIJ undergoes tensile opening above the neutral axis and compressive closing below the neutral axis under the action of external sagging moment M and an axial compressive force N as shown in Fig. 3.2(a). The studs along with intersection joint components above the neutral axis experience tension and below the neutral axis experience compression. These tension and compression components can respectively be modelled as linear springs with stiffness's k_t and k_c. The airframe joint has a rotational opening of ϕ when the joint is subjected to a bending moment and axial force. The axial equilibrium of forces in the FIJ provides

$$\sum F_t - \sum F_c - N = 0 \tag{3.1}$$

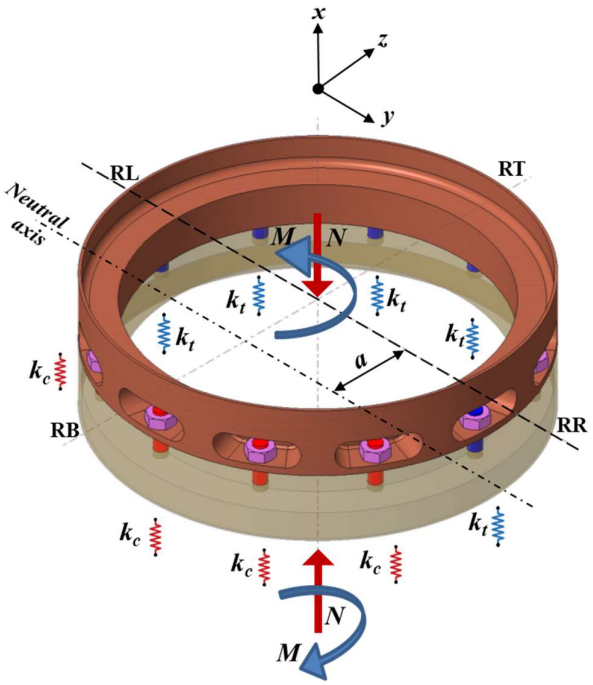

(a) Loadings on a FIJ; and stiffness representation of tension and compression components

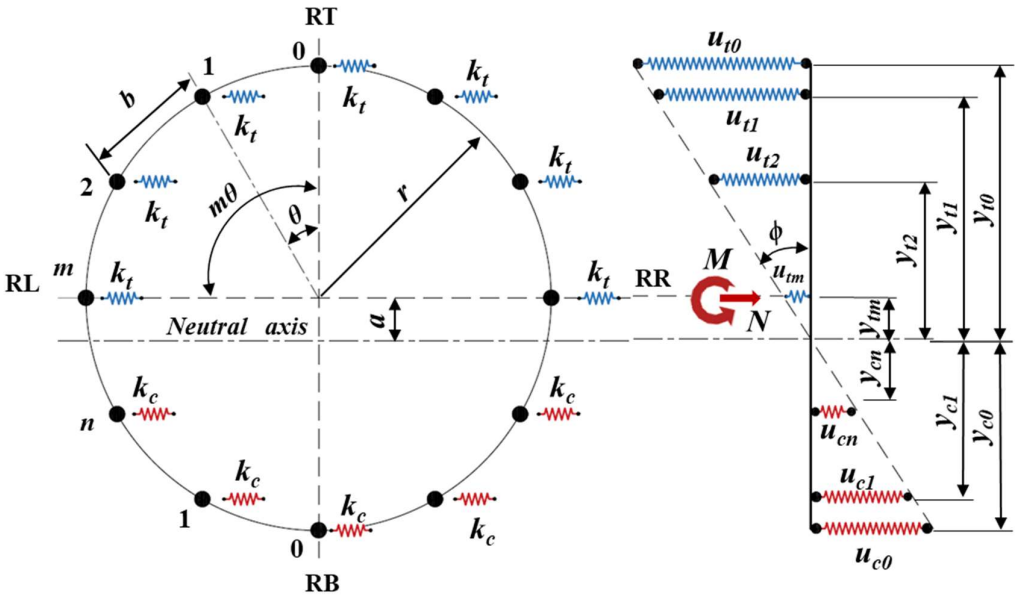

(b) Responses in the FIJ

Fig. 3.2. Mechanical model of the flight intersection joint

Representing the airframe's flight intersection joint stud locations with equivalent springs, the spring force is

$$F_t = k_t\, u_t \tag{3.2}$$

$$F_c = k_c u_c \tag{3.3}$$

where F_t and F_c are respectively the forces in tension and compression components of localised joint represented by equivalent springs k_t and k_c; u_t and u_c are the axial deformation of the springs in tension and compression sides in the FIJ. Referring to Fig. 3.2(b), $2m+1$ and $2n+1$ are the number of studs in the tension and compression sides respectively; r is the pitch circle radius of the studs; a is the distance of the neutral axis from the geometrical horizontal reference RL-RR. The RT is the top reference and RB is the reference at bottom of the FIJ; θ is the angular location of the stud-1 starting from RR reference; y_t and y_c are the linear distances from the neutral axis to the studs in tension and compression sides, respectively; and subscripts to y_t and y_c refer to the stud number.

The axial deformation of the springs is given by

$$u_t = y_t\phi = (r\cos(m\theta) + a)\,\phi \tag{3.4}$$

$$u_c = y_c\phi = (r\cos(n\theta) - a)\,\phi \tag{3.5}$$

The total sum of forces in tension and compression sides are computed as

$$\sum F_t = k_t\,\phi[(r + a) + 2\sum_1^m (r\cos(m\theta) + a)] \tag{3.6}$$

$$\sum F_c = k_c\,\phi\,[(r - a) + 2\sum_1^n (r\cos(n\theta) - a)] \tag{3.7}$$

Substituting Eqs (3.6) and (3.7) into Eq. (3.1), we get

$$k_t\,\phi[(r + a) + 2\sum_1^m (r\cos(m\theta) + a)] - k_c\,\phi\,[(r - a) + 2\sum_1^n (r\cos(n\theta) - a)] = N \tag{2.8}$$

The value of neutral axis location 'a' can be obtained by implicitly solving the Eq. 2.8. The bending moment causing the rotation ϕ of the joint is given as

$$M = M_t + M_c \tag{3.9}$$

where, M_t and M_c are respectively the bending moment of resultant forces on the tension and compression sides and are expressed as

$$M_t = \sum_0^m (F_t\,y_t) = k_t\,\phi\left[(r + a)^2 + 2\sum_1^m (r\cos(m\theta) + a)^2\right] \tag{3.10}$$

$$M_c = \sum_0^n (F_c\,y_c) = k_c\,\phi\left[(r - a)^2 + 2\sum_1^n (r\cos(n\theta) - a)^2\right] \tag{3.11}$$

The joint rotational stiffness K_r of the FIJ can be written using Eqs (3.9 - 3.11) as

$$K_r = \frac{M}{\phi} = k_t\left[(r + a)^2 + 2\sum_1^m (r\cos(m\theta) + a)^2\right] + k_c\left[(r - a)^2 + 2\sum_1^n (r\cos(n\theta) - a)^2\right] \tag{3.12}$$

The JRC of the FIJ is given by

$$JRC = \frac{1}{K_r} \tag{3.13}$$

The JRC of a FIJ can be quantified using Eq. (3.13) if the local tensile and compression component stiffness k_t and k_c are determined separately either through experiments or numerical methods as discussed in the next section.

3.3. Experimental and numerical determination of localised joint stiffness

The component stiffness of a localised segmental joint is analysed by numerical method and validated with the experimental results. The bulkheads and airframe shells are made of aluminium alloy AA2014 in the T6 condition, and studs and nuts are made of EN24 alloy steel. The material properties i.e. the stress – strain curves of AA2014-T6 and EN24 steel are obtained from the tensile tests. These properties are used to simulate the nonlinear material behaviour of the FIJ in numerical simulations. The component stiffness in both tension k_t and compression k_c are determined from the numerical simulation using FEA. The stiffness k_t obtained from FEA in tension is compared with the experimental k_t values to validate the simulation.

3.3.1 Experimental method

Experiments are conducted to evaluate the localised joint stiffness and the material properties needed for numerical simulations.

3.3.1.1 Evaluation of mechanical properties

Specimen geometry

The dog-bone shaped specimens made from aluminium alloy (AA 2014-T6) and EN24 steel (confirming to British Standard BS970-817M40). The specimen's geometric and dimensional details are labelled in Fig. 3.3(a) and given in Table 3.1. The dimensions are chosen as per ASTM E8 standard [53]. Two specimens S1 and S2 were fabricated for each material and the realised specimens are shown in Fig. 3.3(b).

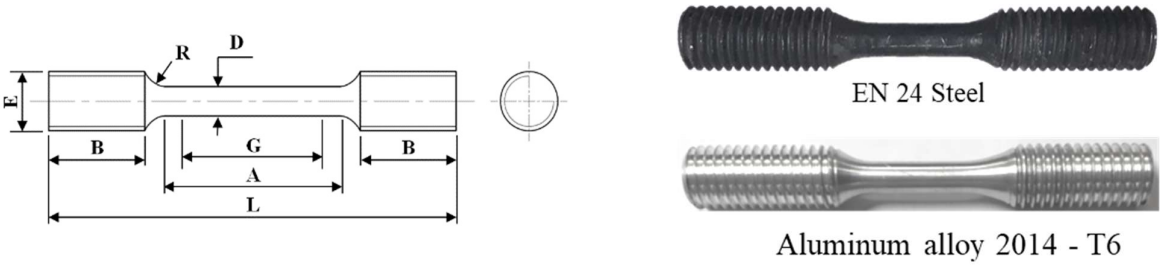

(a) Specimen dimensions (b) Actual specimens

Fig. 3.3. Tensile test specimens

Table 3.1. Dimensions of tensile test specimens (in mm)

Specimen	L	A	G	B	D	R	E
Aluminum alloy (AA 2014 - T6)	85	38	24	20	$6.0^{\pm 0.10}$	6	M12 X 1.75
EN 24 Steel (BS970 - 817M40)	85	34	25	20	$6.25^{\pm 0.12}$	5	M12 X 1.75

Material properties

Tensile tests were conducted for two specimens (S1 and S2) for each material in a universal testing machine to obtain their stress-strain behaviour. Their stress-strain properties are shown in Fig. 3.4. The averaged stress-strain data from experiments are used as material input in FEA to simulate the actual behaviour of the joint. The important mechanical properties derived from the tensile test results are given in Table 3.2.

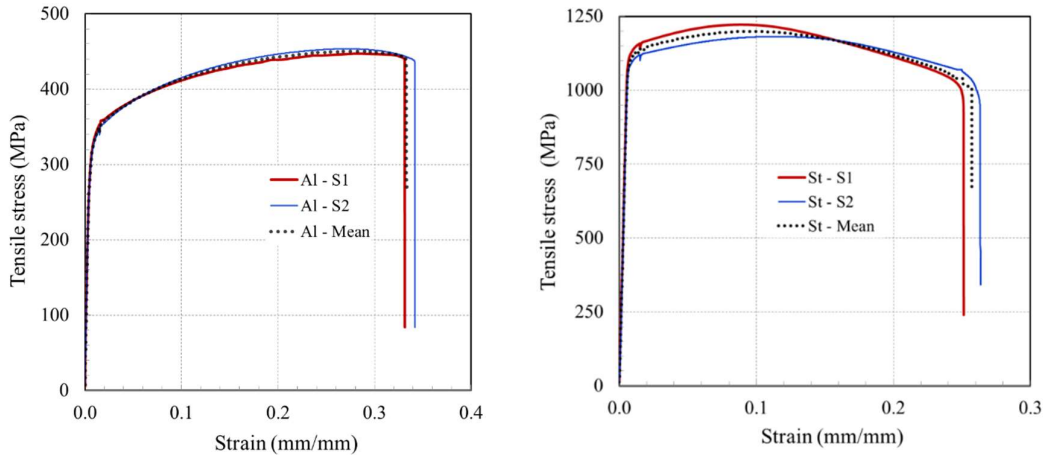

(a) Aluminium alloy AA2014 - T6 (b) Alloy steel EN24

Fig. 3.4. Stress-strain curves obtained from tensile tests

Table 3.2. Material properties from tensile tests

Material	Young's Modulus E (GPa)	Ultimate strength σ_u (MPa)	0.2% proof stress σ_y (MPa)	% Elongation
AA 2014-T6	61.1	447.2	312	10.2
EN24 Steel	187.6	1221.9	1084	18.4

3.3.1.2 Uniaxial experiments on joint specimens

The geometry of the localised stud-pocket type of joint specimen is shown in Fig. 3.5(a). Four numbers of these localised joints were fabricated and are shown in Fig. 3.5(b). Parts-1 and 2 were made from AA 2014–T6 material and the M10 stud and hexagonal nut were made from EN24 steel material. The stud is fastened into Part-2. Part-1 has a clearance hole with a radial slotted recess i.e pocket for inserting the stud and tightening the nut. Tightening torque of 40 Nm was applied on the M10 nut to induce a pretension in the stud.

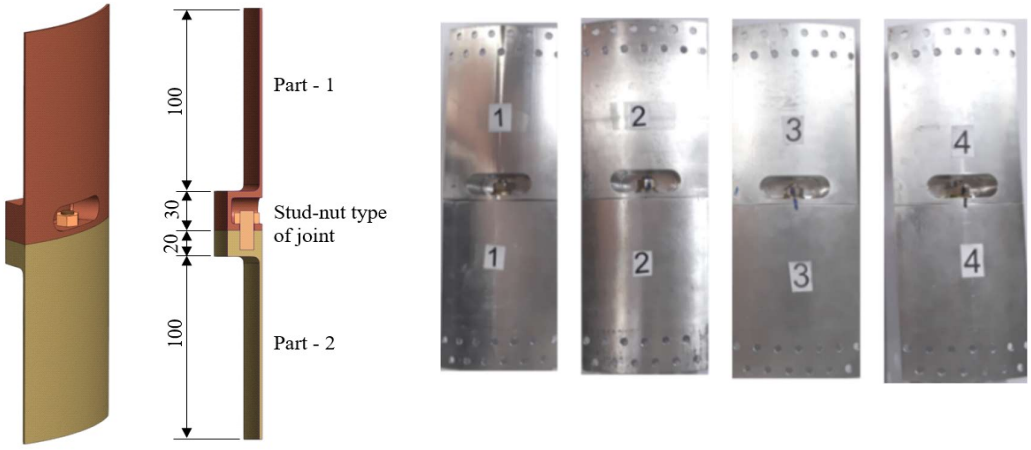

(a) Geometric model (b) Four realized local joints

Fig. 3.5. Geometry of the localised stud-pocket joint

Loading fixtures were made of mild steel and were fastened to Parts-1 and 2 at the free ends to grip the joint specimen during the uniaxial loading experiments. The geometry and the realised model of the four local joints with end attachments for loading are shown in Fig. 3.6.

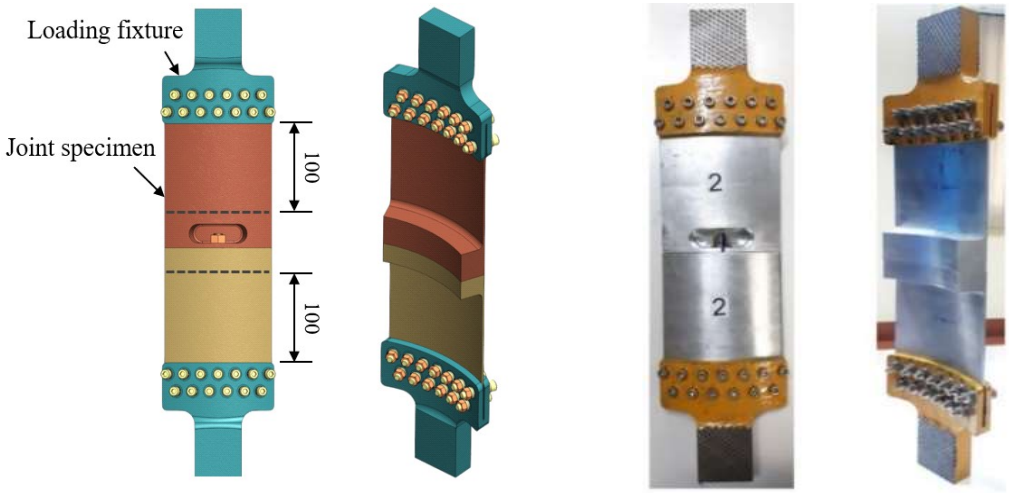

(a) Geometric model (b) Actual joint

Fig. 3.6. Localised joint with end attachments for loading

The joint specimens were subjected to uniaxial loading in a universal testing machine (UTM) as shown in Fig. 3.7(a). The end attachments were gripped in between the top and bottom clamps in the UTM. An L-shaped rectangular aluminium strip is bonded to Part-2 on the joint face at one end. A digital dial gauge is probed on the horizontal flat face of the aluminium strip to measure the joint opening displacement during loading.

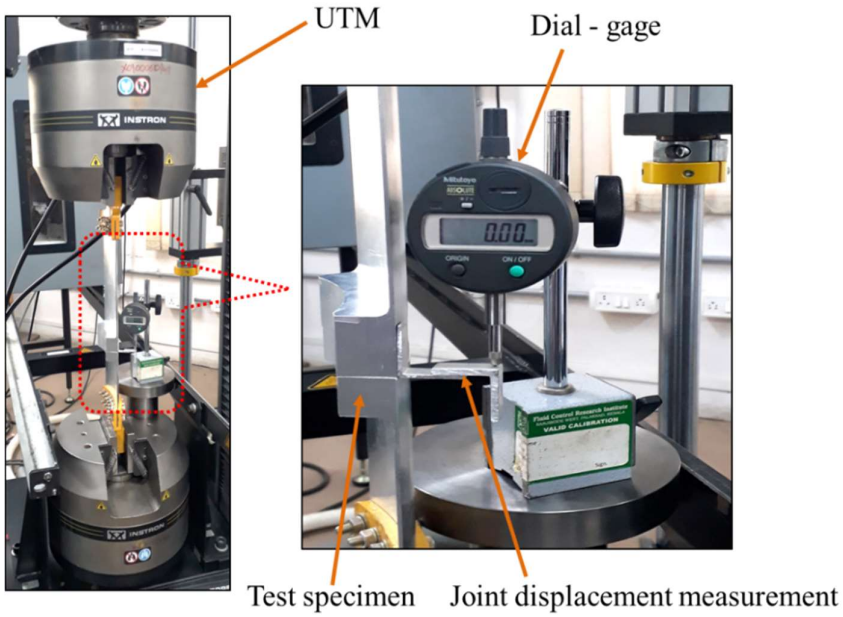

(a) Experimental setup for tensile loading of localised joint

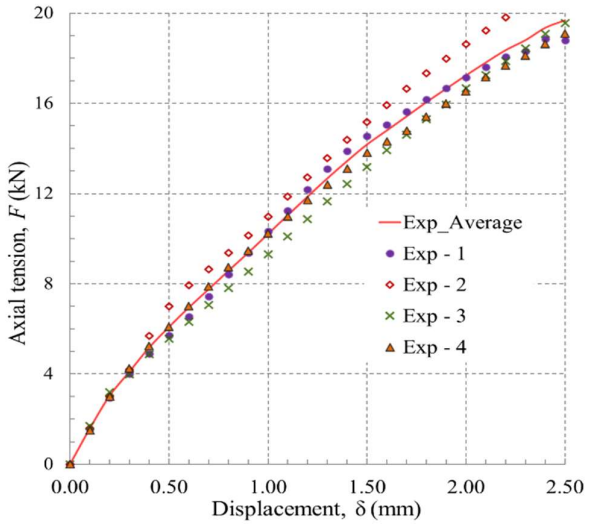

(b) Load-displacement response under tension

Fig. 3.7. Experiments on local joint under tension and their response

3.3.1.3 Determination of component stiffness

Displacement-controlled load is applied in steps of 1mm/ minute up to a maximum displacement of 2.5 mm on the upper fixture. The opening displacement at the joint interface is measured for every 0.1 mm of applied displacement using a digital dial-gauge. The reaction force corresponding to the applied displacement is recorded from UTM. The plot of axial tension experienced by the joint with respect to joint opening displacement δ is shown in Fig. 3.7(b). The average of four experimental results is also plotted. The slope of the initial linear part of the averaged force-displacement curve is the component joint stiffness in tension and is found to be 13.8 kN/mm.

3.3.2 Numerical method

The finite element model with contact interactions and pretension details are shown in Fig. 3.8(a), the loads and boundary conditions are shown in Fig. 3.8(b). The entire model is discretised with 20 node hexahedral elements with an element size of 1 mm using ANSYS Workbench software. As shown in Fig. 3.8(a), the threaded regions between stud and nut, stud and Part-2 are modelled as bonded contacts to simulate the screwed joint. The joints interface between Parts-1 and 2 and the nut surface contacting the flat horizontal face of radial slot in Part-1 are modelled as frictional contacts with a friction coefficient of 0.5. The bottom surface of the FEA model is constrained in all displacement degrees of freedom as shown in Fig. 3.8(b).

FEA simulation was conducted in two load steps. In the first step, a pretension force F_b of 20000N (to simulate the tightening torque of 40 Nm) is applied on the stud surface using pretension element PRETS179 to induce the clamping force on the joint. In the second step, this pretension force is locked and a displacement load is applied on the top surface of Part-1 until the joint tension-deflection behaves nonlinearly. The deformation of the joint under the applied displacement in tension is shown in Fig. 3.8(c). The axial tension experienced by the joint *w.r.t.* the applied displacement δ in the UTM is plotted in Fig. 3.8(d) to measure the joint stiffness in tension k_t.

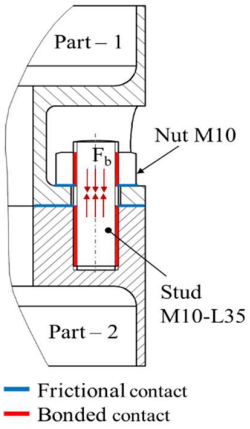

(a) Contact and pretension details

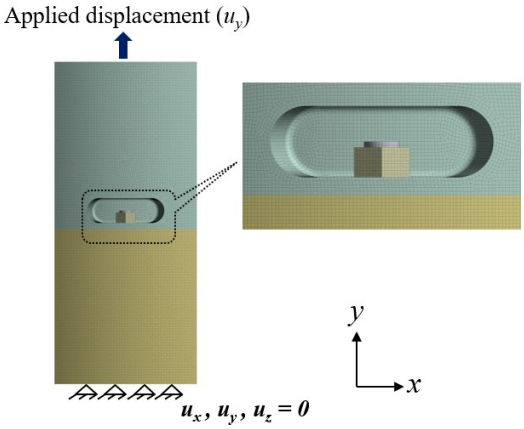

(b) FE model with loading and boundary conditions

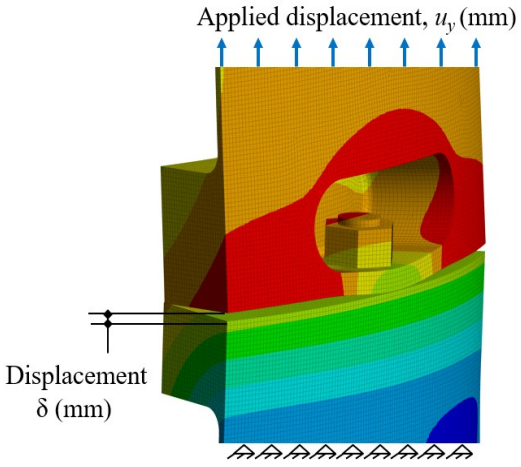

(c) Deformation under tension

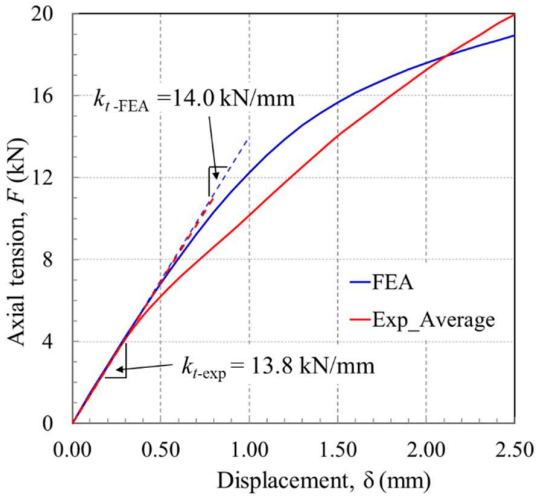

(d) Experiment versus simulation

Fig. 3.8. FEA simulation of localised joint under tension

A similar FEA on the joint is performed in displacement-controlled compression loading to obtain a local joint stiffness in compression k_c. The Fig. 3.9(a) shows the deformation of the joint under compressive displacement, and Fig.3.9(b) illustrates the F- δ compression response wherein the initial slope of the linear range is the compression stiffness k_c, is measured as 50.0 kN/mm.

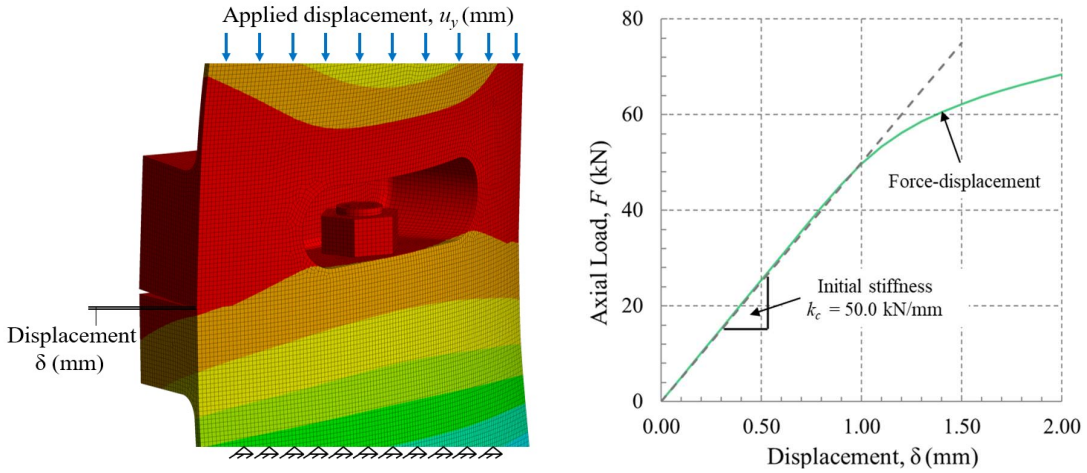

(a) Deformation of the joint under compression

(b) Force-displacement under compression

Fig. 3.9. FEA simulation of localised joint stiffness under compression

3.3.3 Comparison of localised joint stiffness from FEA and experiments

The averaged load-displacement (F- δ) result from the four experimented local joint specimens is plotted along with results from FEA simulation in Fig. 3.8(d). As shown in the figure, F- δ response is linear up to 0.4 mm of displacement for all the experimented specimens and afterwards the curves behave nonlinearly. The initial slopes of these F- δ curves represent the axial joint stiffness in tension k_t. The axial joint stiffness obtained from FEA simulation is 14.0 kN/mm against the experimentally determined stiffness of 13.8 kN/mm. A close agreement is observed between the results of FEA and experiment for the tensile stiffness of the localised component joint stiffness.

3.4. Computation of JRC of FIJ from theoretical model

The complete flight intersection joint having an airframe diameter of 300mm with eight numbers of M10 stud-pocket-nuts is considered as an illustrative example as shown in Fig.3.10(a). The bending moment M is applied matching the first yield moment M_y of the airframe material.

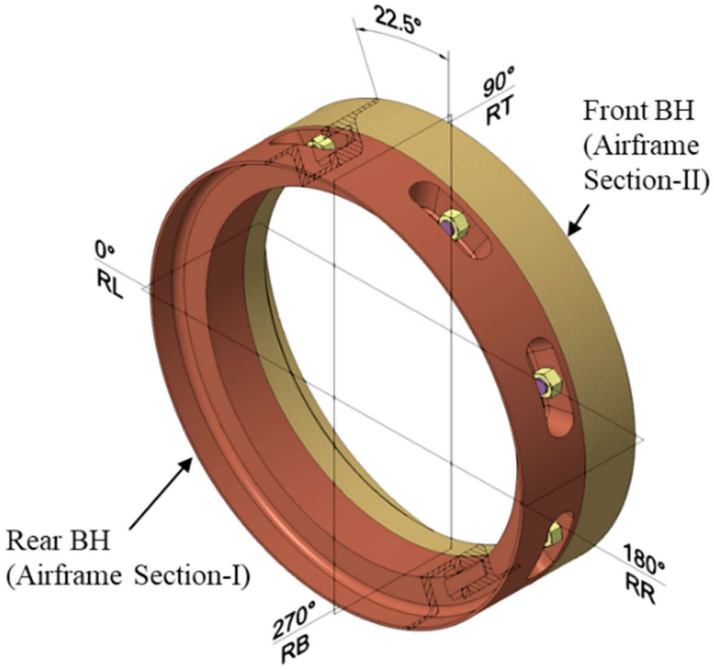

Fig. 3.10. Geometry of a typical FIJ connecting airframe sections-1 and 2

The value of neutral axis location 'a = 0' here due to the absence of axial force. Here, m = 4, r = 125mm and θ = 45^0. The JRC from theoretical model is computed using Eq. (3.13) wherein the local component joint stiffness evaluated numerically is considered i.e. local joint stiffness in tension k_t = 14.0 kN/mm and compression k_c = 50.0 kN/mm are adopted. The calculated JRC from the theoretical model is 0.231 rad/MNm as shown in Fig. 3.11 w.r.t the variation in ratio of applied moment normalised by the first yield moment.

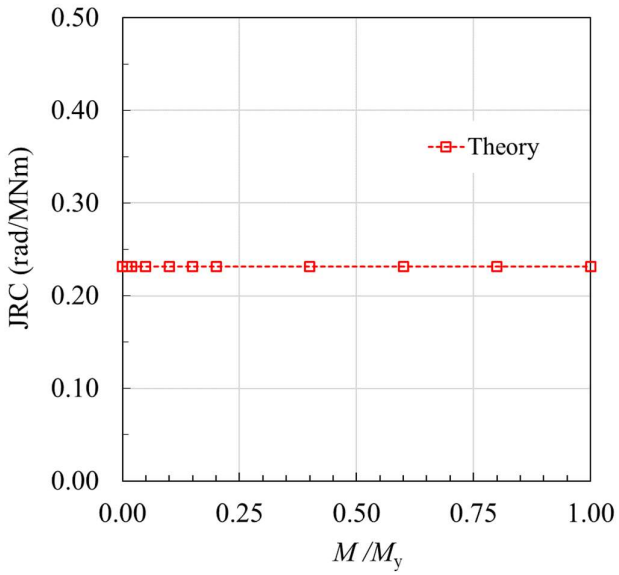

Fig. 3.11. Computed JRC resulting from theoretical model

3.5. Summary

Flight intersection joints (FIJs) integrate individual airframe sections in a launch vehicle and is characterised by the joint rotational compliance (JRC). This JRC is adopted to model the dynamic characteristics of the launch vehicle. The JRC is often quantified through extensive experiments. This chapter has brought out a theoretical model for JRC of a stud-pocket type of a FIJ. This JRC model of the FIJ relies on localised component joint stiffness. The localised joint stiffness has been determined through experiments and numerical simulations where both methods resulted in close values. The JRC has been predicted *w.r.t.* increase in applied bending moment using the theoretical model for a typical FIJ having eight equi-spaced M10 studs. This JRC model will be validated with numerical and experimental methods in subsequent chapters.

Chapter - 4

Numerical Simulation of JRC of a Tension Type FIJ

4.1. Introduction

The joint rotational compliance of a flight intersection joint computed through the theoretical model discussed in the previous chapter is validated through the FEA based numerical simulation presented in this chapter. A full scale FEA model of a typical FIJ is modelled with appropriate boundary conditions and contact definitions. The moment loads as proportion of the first yield moment of the airframe material is applied incrementally until the ratio of these two moments reaches unity. The displacements or the axial openings at the interface of the FIJ along the circumference is measured through the analysed model. The measured openings are used to compute the JRC. This is further compared with that calculated from theoretical model. To understand the behaviour of FIJ on JRC, different studies are conducted through the numerical simulations. The effect of pre-tightening or pre-torquing on the joint is analysed. Parametric studies are conducted by varying the number and size of studs to find their best combination to achieve a minimal JRC. The influence of various geometric parameters in the joint are independently studied to assess their impact on the JRC of the FIJ. The effect of airframe diameter on JRC is analysed. In addition to the above, the estimation of JRC under the combined loading of bending moment and axial force is elucidated. The details are presented in this chapter.

4.2. Numerical Modelling of JRC of FIJ

The complete flight intersection joint having an airframe diameter of 300mm with eight numbers of M10 stud-pocket-nuts is modelled as shown in Fig. 4.1(a). This FIJ is discretized with 20 node hexahedral elements with an element size of minimum of 1 mm. The rear end of the front bulkhead of the airframe Section-II with protruding studs in front is constrained in all three displacement degrees of freedom. The rear bulkhead of airframe Section-1 having pockets to receive the studs is subjected to a bending moment. The loads and boundary conditions on the FIJ are shown in Fig. 4.1(b). The contacts between the studs and bulkhead interfaces, stud-nut and nut and contacting bulkhead faces in the pocket are modelled as per the details explained in Fig. 3.8(a) in Chapter-3. The material properties of FIJ i.e. airframe, studs and nuts obtained

from tensile tests detailed in Chapter-3 are used as inputs in the present numerical simulation. The bending moment M is applied proportionally in steps until the first yield moment M_y of the airframe is reached.

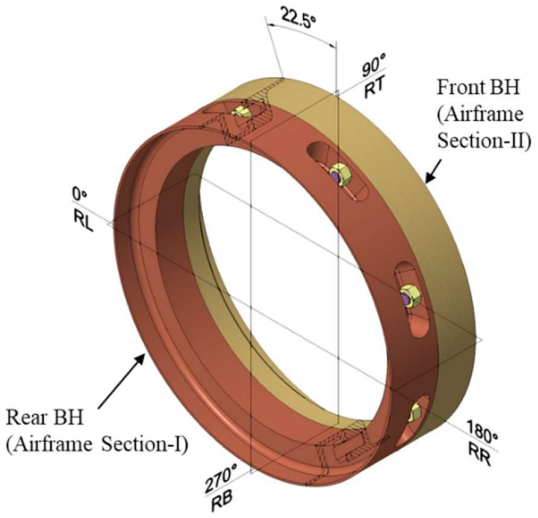

(a) Details of FIJ connecting airframe sections-1 and 2

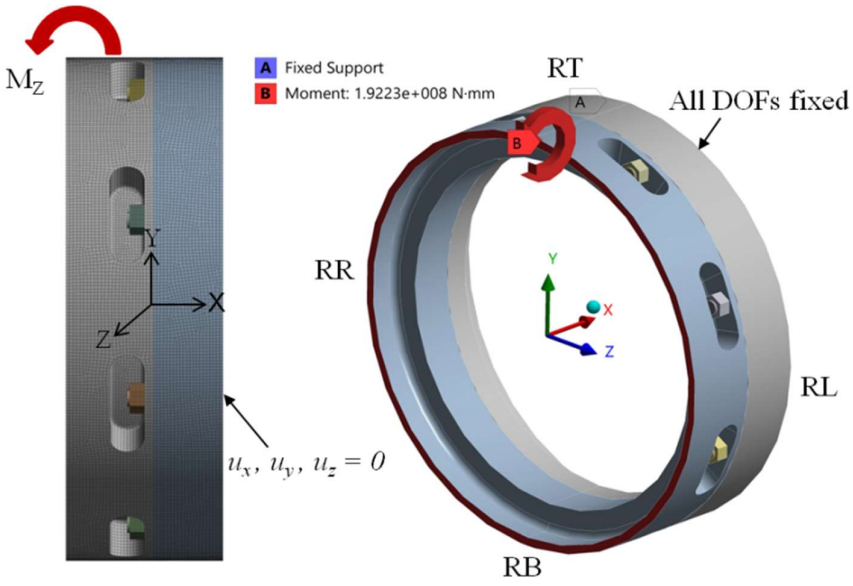

(b) FEA model with loads and boundary conditions

Fig. 4.1. Geometry and FEA model of a typical FIJ

The axial displacements at the joint are measured after the analysis. The plot showing the axial opening at RT (i.e. the reference at top of FIJ) and RB (i.e. the reference at the bottom of the FIJ) references due to the application of bending moment is shown in Fig. 4.2(a). A

maximum opening of 0.65 mm is observed at RT location and 0.01 mm compression is observed at RB location. The variation of axial opening along the circumference of the airframe at the plane of the FIJ for the applied M/M_y starting from 0º at RL, 90º on RT, 180º on RR and 270º on RB to 360º on RL is shown in Fig. 4.2(b). Although a maximum joint opening of 0.65 mm is observed at RT orientation, the opening was negligible at locations where the joint is fastened with a stud. From the RR to RL region, the joint undergoes compressive displacement up to 0.01 mm at the RB zone.

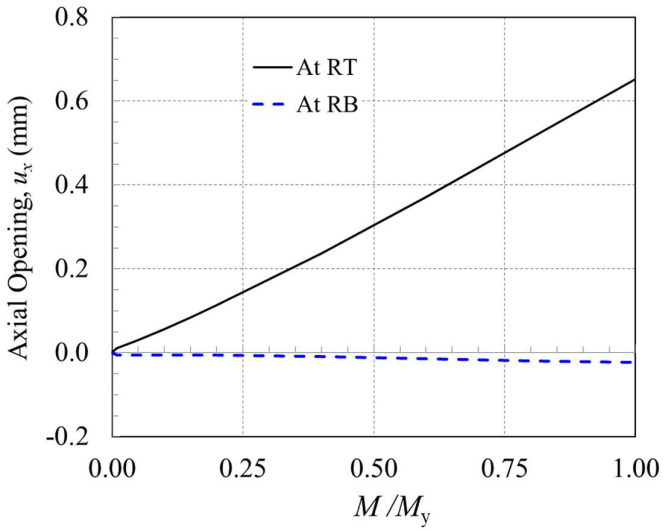

(a) Axial opening at RT and RB with applied moment

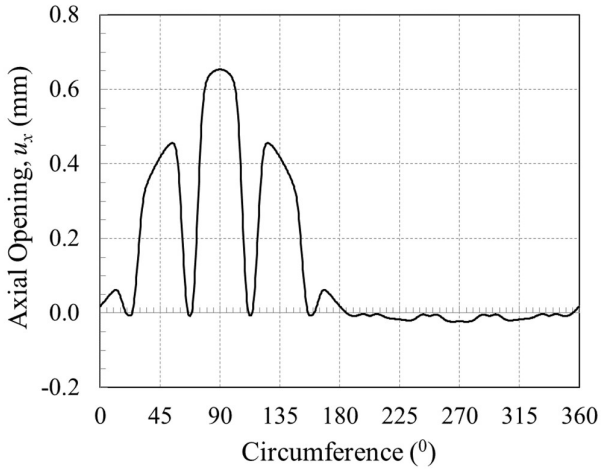

(b) Axial opening along circumference starting from RL at M/M_y =1 (see Fig.4.1 (a))

Fig. 4.2. Axial opening in FIJ under applied bending moment

The axial opening u_x shown in Fig. 4.2 refers to the axial deformation of springs equivalent of stud-nut represented as u_t in tensile side and u_c in compression side respectively above and below the neutral axis shown in Fig. 3.2(b). The value of neutral axis location 'a = 0' here due to the absence of axial force. Using Eq. (3.4), and taking m = 4, r = 125mm and θ = 45^0, the rotation of the joint ϕ can be calculated from

$$\phi = \frac{u_t}{r\cos(m\theta)} \tag{4.1}$$

The JRC of the FIJ from FEA simulations is given by

$$JRC = \frac{\phi}{M} \tag{4.2}$$

For every increment in applied bending moment M, value of JRC can be computed.

4.3. Comparison of theoretical solution with FEA simulation

The JRC from the theoretical model is computed using Eq. (3.13) wherein the local component joint stiffness evaluated numerically (as explained in Chapter-3) is considered i.e. local joint stiffness in tension k_t = 14.0 kN/mm and compression k_c = 50.0 kN/mm are adopted. The JRC from FEA simulation is obtained from Eq. (4.2). The comparison of JRC resulting from the theoretical model and FEA simulations against the applied bending moment ratio is shown in Fig. 4.3. It can be observed that the JRC remains constant for a definite type of FIJ based on theoretical model and is independent of the applied load. This constancy qualifies this JRC to be considered as a joint's characteristic property. An ideal or a preferred joint should possess very less joint flexibility i.e. JRC and very high joint rotational stiffness K_r. Although a small variation is found in FEA result of JRC, it is in close agreement with the JRC obtained from the theoretical model, thereby validating the accuracy of the theoretical model.

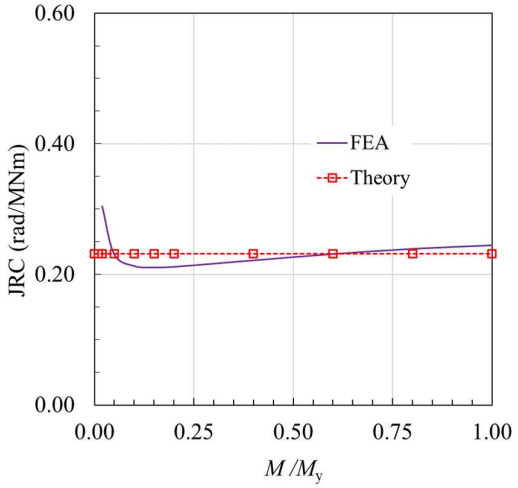

Fig. 4.3. Comparison of JRC resulting from theoretical model and FEA simulations

4.4. Effect of Pre-tightening on JRC

Numerical studies were conducted to study the effect of stud pre-tension on the rotational compliance of the FIJ. The pretension was applied to the stud as explained in Chapter-3 and shown in Fig. 3.8(a). Figure 4.4 shows the plot of percentage difference between JRC with pre-tightening (JRC_{PT}) and JRC with no pre-tightening (JRC_{NPT}) *w.r.t.* JRC_{NPT}. The JRC_{PT} gradually decreases from close to 30% at initial load to about 10% at the maximum yield moment. This indicates that the bolt preload decreases the rotational compliance of the joint, which is highly desirable. The pre-tightening always enhances the JRC and is hence recommended in all FIJs. Apart from reduction in JRC of the FIJ, the pre-tightening additionally delays the vibration loosening of the joint.

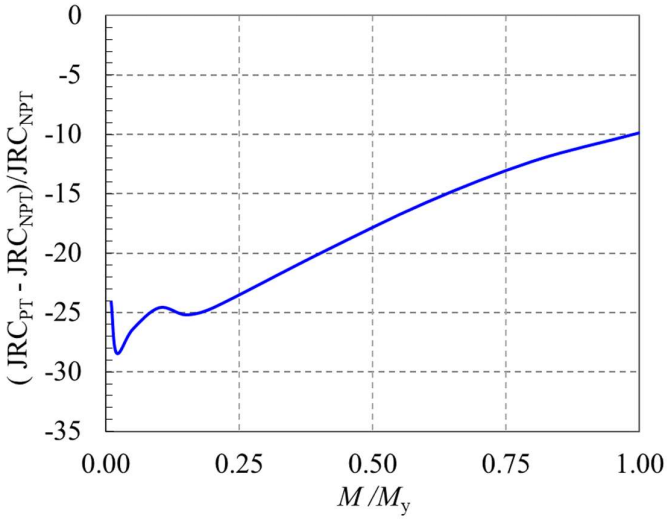

Fig. 4.4. Effect of pre-tightening on JRC of FIJ

4.5. Studies to enhance JRC

Different studies were carried out to achieve minimal JRC which can be beneficial during the initial design stage of a FIJ. The studies involved three practically adaptable approaches. One is the study on the effect of the number of studs for a given nominal size of the stud in the FIJ, the second approach is to examine the effect of size of studs for the given number of studs, and the third is the effect of variation in both the number and size of the studs.

4.5.1 Variation in the number of studs

The increase in number of the similar metric size of studs for a FIJ has a profound effect on the JRC. Fig. 4.5(a) shows the variation of axial opening for a different number of M10 studs with an increasing moment load. The plot clearly shows that an increase in the number of studs decreases the axial opening. A maximum opening of 2.3 mm is observed for 4numbers of M10 studs, and it reduces to nearly half around 1.1 mm for 6 numbers of studs. The axial opening for 8 and 10 numbers of studs is 0.52 mm, and a slightly lower value of 0.51 mm for 12 numbers. The plot of the axial opening along the circumference of the FIJ with an increase in the number of M10 studs is shown in Fig. 4.5(b). A positive opening displacement was observed from 0^0 at RL to 180^0 at RR, with a maximum opening occurring in RT at 90^0 for the varying number of studs. In the region RR-RB-RL from 180º to 270º and from 270 º to 360º, the entire axial opening is almost constant, negligible and is compressive as the studs fall below the neutral axis of the FIJ during loading. In all the cases, from RL to RR, the opening is close to zero at locations of studs. Figure 4.5(c), shows the variation of JRC for different number of studs. As the number of studs increases, the value of JRC decreases linearly up to 8 number of M10 studs. From 8 to 10 numbers of studs, the value of JRC remains almost constant and decreased slightly for 12 numbers of M10 studs. This study reveals that the increase in the number of studs of a given stud size will certainly improve the JRC.

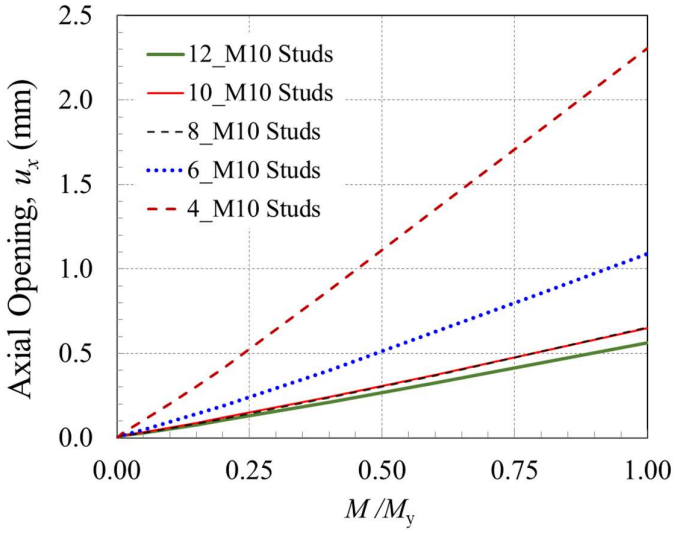

(a) Axial opening at RT with an applied moment

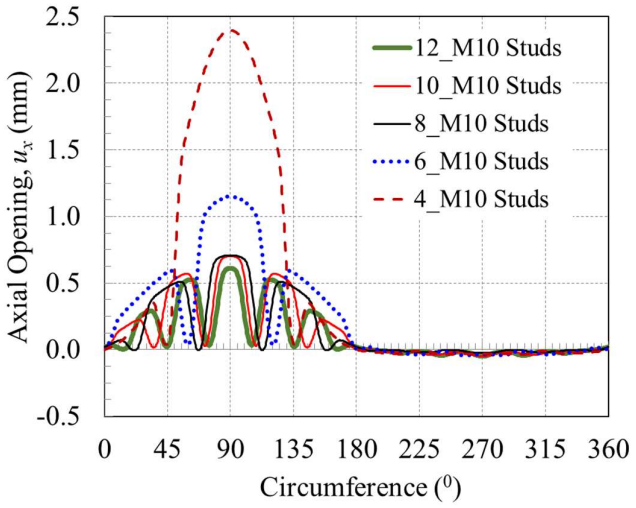

(b) Axial opening along circumference starting from RL at M/M_y =1 (see Fig. 4.1(a))

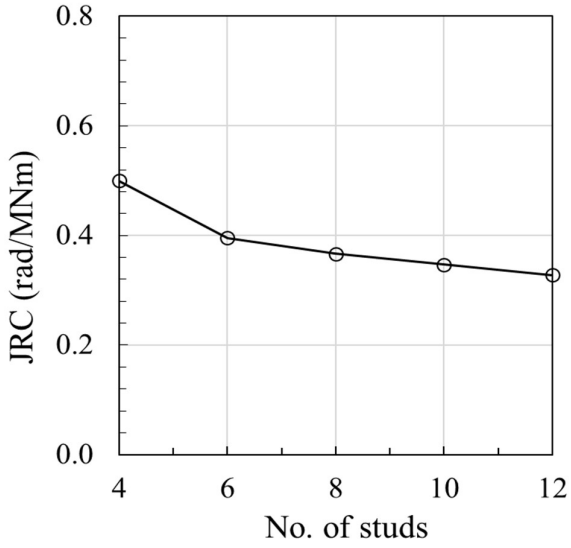

(c) JRC *w.r.t.* number of studs

Fig. 4.5. Effect of variation in the number of M10 studs on joint opening and JRC

4.5.2 Variation in metric size of studs

The variation in different metric sizes (M6 to M12) of a given number (12) of studs can influence the axial opening and therefore the JRC of the FIJ which is investigated here. Figure 4.6(a) shows a linear increase in axial opening under increasing bending moment for 12 numbers of a given metric size of the stud. The axial opening decreased with an increase in the size of the studs. A maximum opening of 0.66 mm was observed with M6 studs and a minimum of 0.56 mm for M12 studs. The axial opening for the remaining M8 and M10 studs is between 0.56 and 0.66 mm. The difference between the maximum and minimum opening is 0.1 mm, and the axial opening in FIJ has less influence on the different metric sizes of studs.

The plot of the axial opening across the circumference of FIJ for the different metric sizes of studs is shown in Fig. 4.6(b). As previously seen in Fig. 4.5(b), a positive opening is observed from 0º to 180º i.e. from RL to RR via RT and compressive closing is observed from RR to RL via RB i.e. from 180º to 360º. The maximum and minimum openings of 0.7mm and 0.55mm were respectively observed with M6 and M12 studs. The effect of variation in metric size of studs from M6 to M12 for the given 12 numbers of studs on JRC is shown in Fig. 46(c). It is observed that the increase in the metric size of studs could decrease the JRC very marginally.

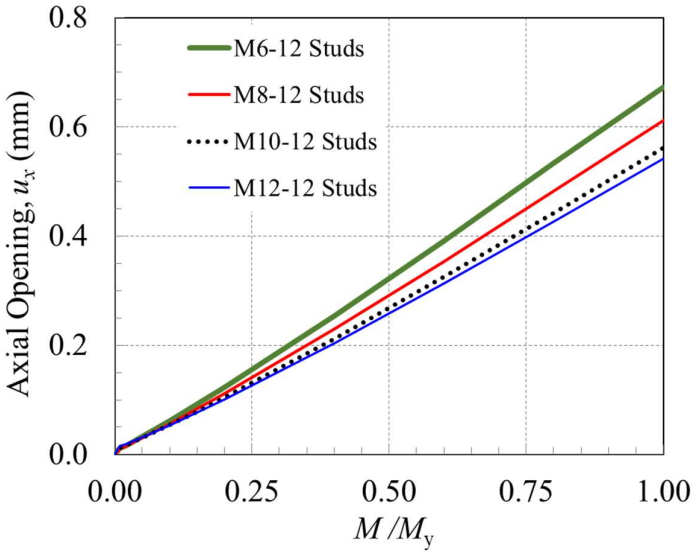

(a) Axial opening at RT with an applied moment

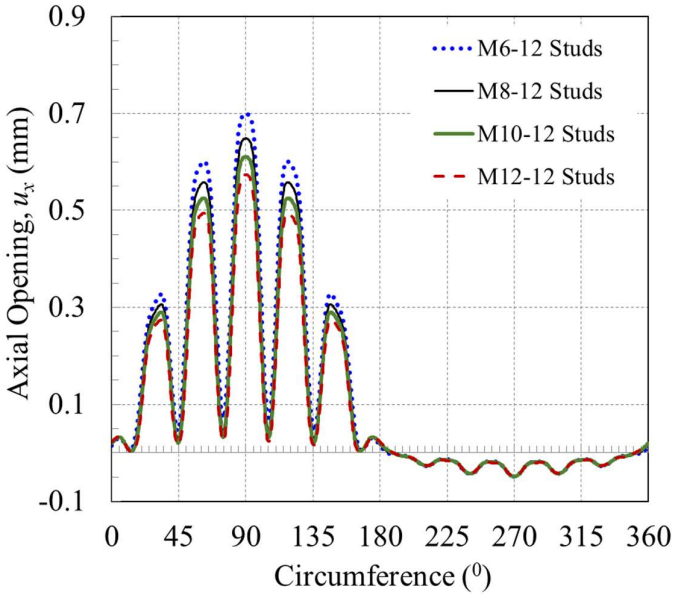

(b) Axial opening along circumference starting from RL at M/M_y =1

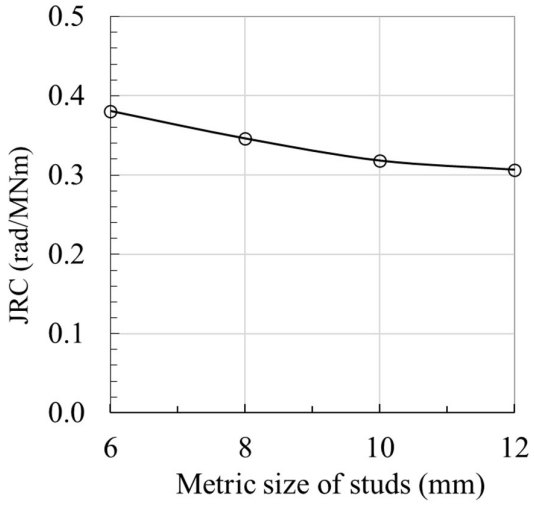

(c) JRC *w.r.t.* size of studs

Fig. 4.6. Effect of variation in metric size of studs on the joint opening and JRC

4.5.3 Variation in the number and size of studs

Variation in both the number and size of studs on JRC is investigated and shown in Fig. 5.7(a). There is 71.8% and 52.7% decrease in JRC for the FIJ having respectively eight and six numbers of M10 studs as compared to FIJ with four numbers of M10 studs. There is no much variation observed in JRC from 8 to 12 numbers of M10 studs. Twelve numbers of M8 studs give better JRC as compared to ten numbers of M10. As a whole, 12 numbers of M12 studs gives the least JRC and highest joint rotational stiffness (JRS) i.e K_r (as seen in Fig. 4.7(b)) for the different combination of number and metric size of studs studied. Therefore, for the typical airframe diameter of 300 mm considered, adopting 12 numbers of M8 or M10 studs proves to be an optimum solution to achieve the minimum possible JRC and maximum JRS.

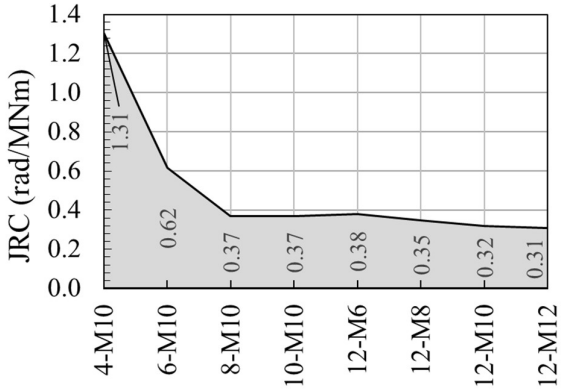

(a) Variation of JRC

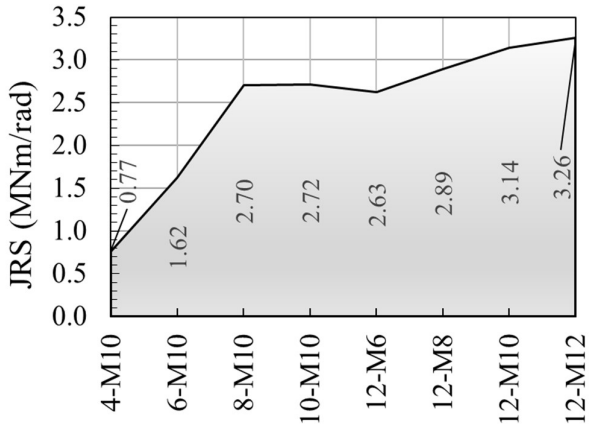

(b) Variation in JRS

Fig. 4.7. JRC and JRS variation *w.r.t.* variation in the number of studs and size of studs

4.5.4 Variation in stud-pocket geometric parameters

Several geometric parameters decide the FIJ's internal dimensions and width. These parameters can be expressed in terms of airframe shell's thickness. These geometric parameters are shown in Fig. 4.8(a). Increase in t_2 decrease the available volume inside the FIJ which will limit the configuration of internal subsystems within the flight. Increase in b_2 and b_5 increases the overall width of the FIJ which will increase the mass of the FIJ. But detailed parametric studies involving variation of several geometric parameters revealed the dependency of only two critical thickness parameters such as t_3 and t_5 on JRC. The variation of these critical parameters on JRC is shown in Fig. 4.8(b) which highlights that increase in these two parameters yield a beneficial and an exponential decrease in JRC.

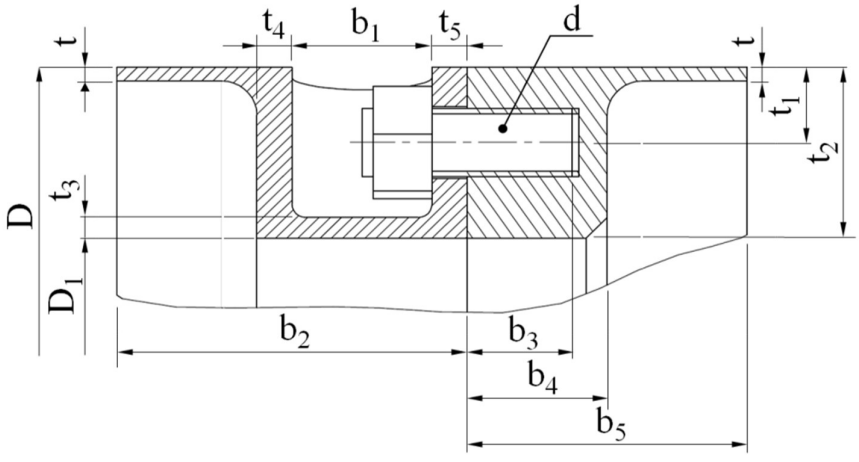

(a) Detail of stud-pocket joint

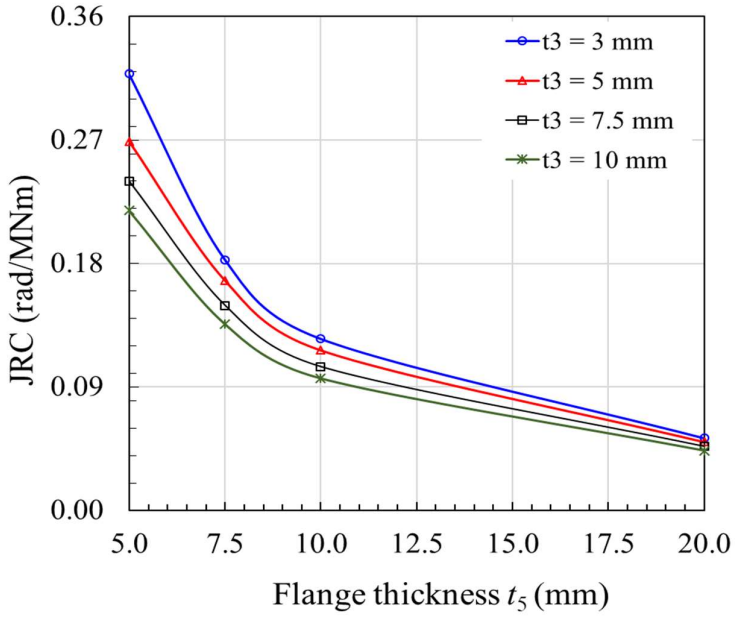

(b) Effect of stud-pocket geometric parameters

Fig. 4.8. Effect of stud-pocket geometric parameters on JRC of FIJ

4.6. Effect of FIJ's diameter on JRC

The effect of variation in diameter of airframe, circumferential distribution in studs and number of studs are analysed through FEA based numerical simulations and compared with theoretical predictions for the base or the reference airframe diameter i.e. 300mm. Three different cases are considered in studying the effect of variation in diameter of FIJ on its JRC as given in Table 4.1.

Table 4.1. Different cases in varying diameters of FIJ

Case	Diameter and loading particulars
1	FIJ with 8 numbers of M10 studs subjected to $0.2M_y$ (i.e. 20% of airframe's respective first yield moment).
2	FIJ with 8 numbers of M10 studs subjected to a constant bending moment M (say, $M = 0.2M_{y\ of}$ 300mm FIJ).
3	FIJ with studs positioned at constant arc length similar to Ø 300 and subjected to $0.2M_y$ (i.e. 20% of airframe's respective first yield moment).

The axial opening along circumference of the FIJ *w.r.t.* the variation in airframe diameter in Case-1 is shown in Fig. 4.9. This shows that when the number and size of studs are

same (here 8 numbers of M10), and when FIJ is loaded up to 20% of the respective yield moment, the axial opening reduces significantly with increase in airframe diameter. This in turn results in corresponding decrease in JRC as shown in Fig. 4.10(a). But the difference in JRC between 300mm and 500mm airframe diameters is very small as compared to that in 1000mm due to considerable variation in the airframes second moment of area in the latter's case.

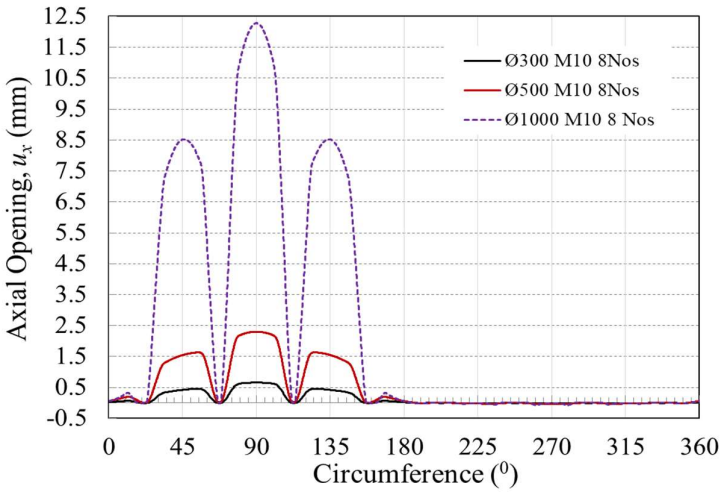

Fig. 4.9. Axial opening along circumference of the FIJ *w.r.t.* variation in airframe diameter under Case-1

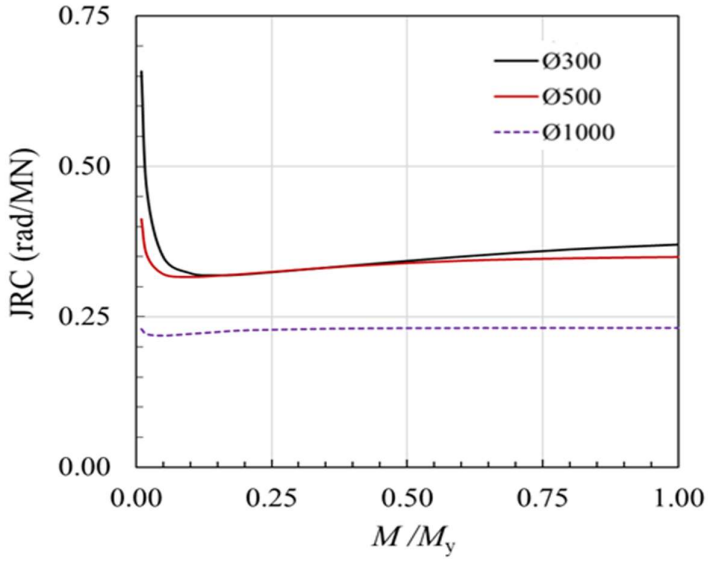

(a) JRC of the FIJ *w.r.t.* variation in airframe diameter in Case-1

On the other hand, in Case-2 situation when the three different diameters considered here are subjected to the same bending moment, the JRC decrease considerable with increase in airframe diameter as shown in Fig. 4.10(b). In Case-3 situation, where the arc-length between studs are maintained same as that existing in diameter 300mm airframe for the 500mm and 1000mm airframe as well, the number of studs increases which in turn cause substantial decrease in JRC as shown in Fig. 4.10(c). Further, improvements in JRC considering 300mm diameter of airframe as baseline reference is shown in Fig. 4.11. These three cases highlight that the design recommendation needs to align with Case-3 situation to achieve highest possible joint stiffness.

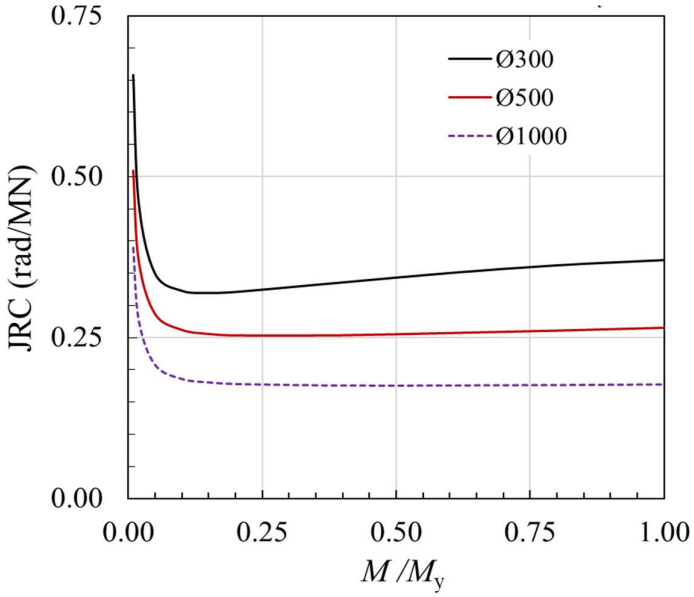

(b) JRC of the FIJ *w.r.t.* variation in airframe diameter in Case-2

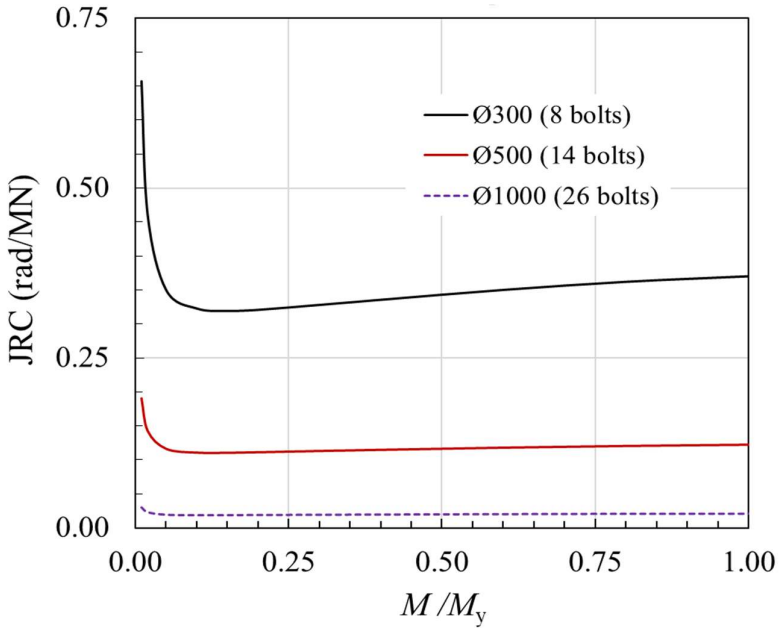

(c) JRC of the FIJ *w.r.t.* variation in airframe diameter in Case-3

Fig. 4.10. JRC of the FIJ *w.r.t.* variation in airframe diameter three different Cases

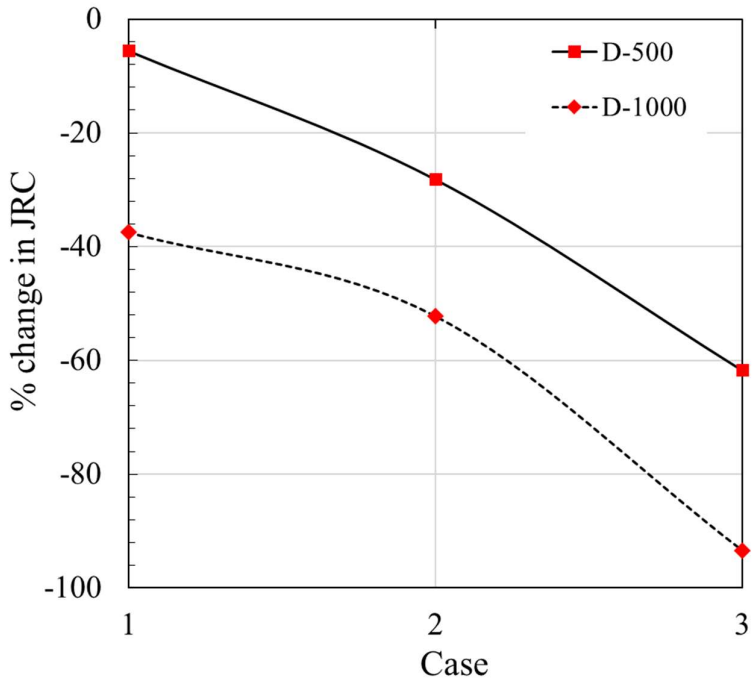

Fig. 4.11. Improvement of JRC w.r.t. to 300mm airframe diameter

4.7. Summary

The JRC has been predicted *w.r.t.* an increase in applied bending moment using the theoretical model for a typical FIJ having eight equi-spaced M10 studs. The FIJ has been modelled numerically with appropriate contacts, boundary conditions and loadings and its JRC has been determined through FEA simulations. The predicted JRC from the theoretical model agreed very well with the results from the FEA simulations. Further, the effect of pre-tightening of studs, variation in number of studs, variation in metric size of studs and their combinations, variation in geometric parameters of FIJ, variation in airframe diameters and effect of combined bending moment and axial force on JRC have been investigated to understand their influence on the JRC. The following three key inferences can be summarised from the latter investigations.

- Pre-tightening of studs enhances the JRC to an extent of 30% to 10% when loading is increased from no load to the first yield moment.
- An increase in number of studs for a given stud size could enhance the JRC significantly as compared to the increase in metric size of studs for the given number of studs.
- Higher numbers with lesser size of stud has enhanced JRC when compared with fewer numbers of higher sizes of studs. Hence, the FIJs with more number of studs are recommended when compared with a lesser number of studs for the same stud size.
- Increasing the number of studs with increase in airframe diameter enhances the JRC of the FIJ.

Chapter 5

Experimental Determination of JRC for a Tension Type FIJ

5.1 Introduction

The estimation and quantification of JRC for a FIJ is a very vital property. The previous chapters elucidated the methodology of obtaining the joint stiffness numerically by using a localized segmental joint and substituting it in theoretical computation of JRC. Based on this numerical procedure, JRC of full FIJ is obtained. The numerical results of JRC of full FIJ are validated by experiments by realising the FIJ. A detailed experimental setup needs to be designed for conducting the experiment based on the numerical model of FIJ. The experimental set up constitutes of flight worthy airframe and fastening materials, ground support structures, test rig for applying load, instrumentation devices like force transducers for load, LVDTs for displacement measurement connected to a data acquisition system. The experimental FIJ specimen should be designed in such a way that the true load is transferred at the joint. The actual airframe with FIJ should have an additional loading component for the application of bending load corresponding to the bending moment and also a base plate attachment for fixing of the airframe to the support structure. The application of load at the FIJ to simulate the bending moment from the test rig that can deliver the required control loading has to be planned and arranged. The system should allow for a gradual application of load using a loading test rig with proper fluid flow control. A suitable fixture for mounting the loading actuator need to be designed including its mounting to support structure so that the reaction due to the load application is resisted by the fixture and support structure and in turn the true load is applied at the FIJ. Proper calibrated instruments for measuring the opening displacement using LVDTs, force transducers, data acquisition system are important prior to the conduct of the test. The JRC of FIJ is computed based on the opening displacement obtained from the experiments under the load and is compared with the numerical result for validation.

5.2 Design and Analysis of Experimental Setup

In order to manufacture the experimental setup to conduct the experiment to quantify JRC of a tension type FIJ, it is very important to primarily conceptualise, design and analyse the experimental setup so that the FIJ experiences the actual joint load. This process helps in

manufacturing an appropriate setup which will meet the objectives of the planned experiments. Therefore, the design and analysis of the experimental setup is presented in this section.

5.2.1 Design of experimental setup

The slot-nut type FIJ for conducting the experiment is designed simulating its closeness to the typical flight vehicle airframe section assembly as shown in Fig. 5.1(a). Airframe of diameter 300mm is chosen. The joint design consists of an airframe bulkhead with eight numbers of M10 size studs at one end (i.e. at front bulkhead of airframe Section-II) which enters into the neighbouring airframe bulkhead having eight pockets and stud entry holes (i.e. at rear bulkhead of airframe Section-I) and clamped with nuts as shown in Fig. 5.1(a). The dimensional details of the assembly is shown in Fig. 5.1(b). The dimensional details of experimental FIJ is given in Fig. 5.1(c). For the airframe Section-II, only the front bulkhead with studs is adopted. The joint is designed considering the actual airframe shell thickness i.e. airframe Section-I having slot or pocket has a shell thickness of 2mm up to a length of 180mm. The other end of the joint in Section-I is integrated with an additional loading ring for applying lateral force to simulate the bending moment on the FIJ specimen. Fig. 5.1(d) shows the detailed exploded view of experimental FIJ. This additional loading ring is made of C40 steel and is assembled on the loading side of the airframe i.e. Section-I front end using 12 numbers of M8 CSK screws as shown in Fig. 5.1(d).

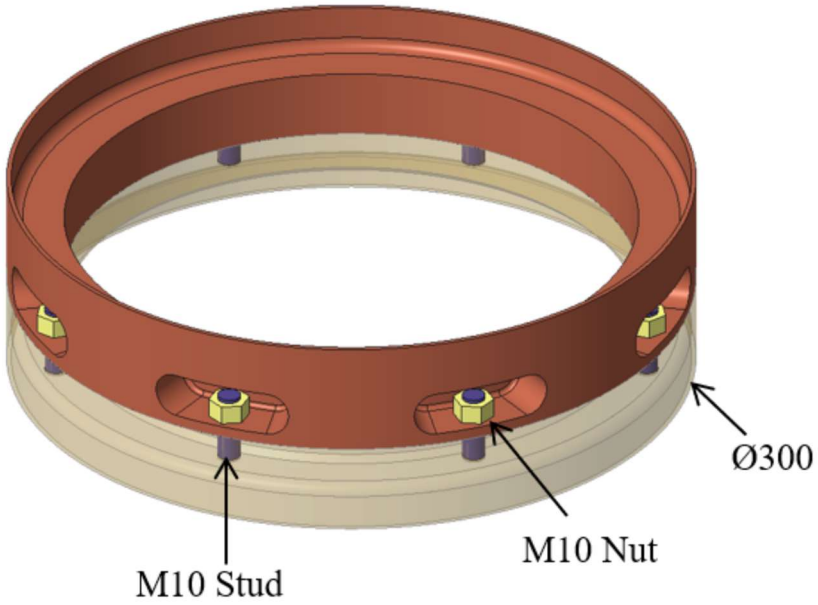

(a) Typical FIJ Assembly

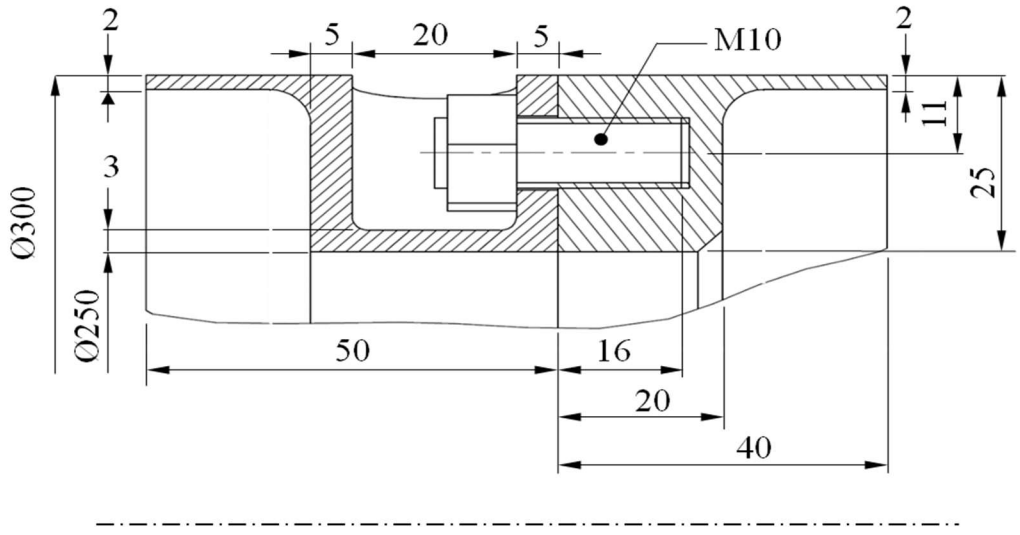

(b) Dimensional details of FIJ Assembly

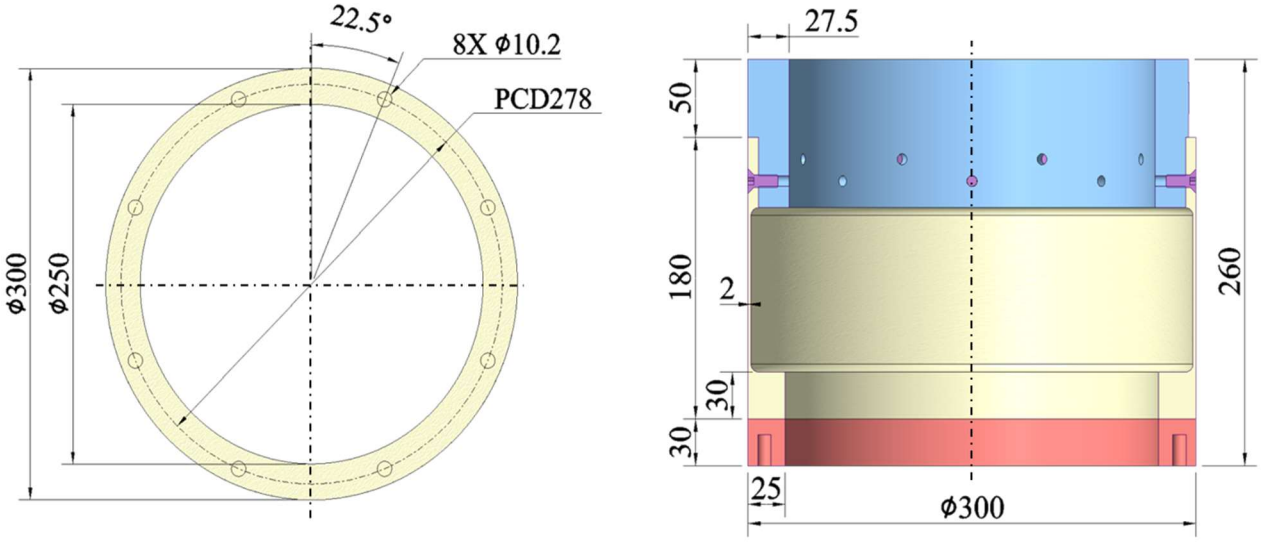

(c) Dimensional details of experimental FIJ

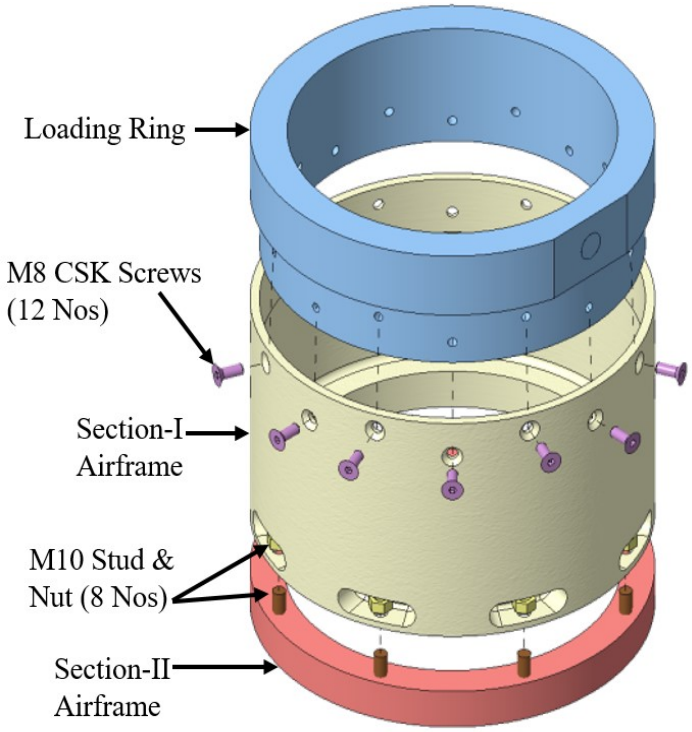

(d) Exploded view of Experimental FIJ

Fig. 5.1. Experimental FIJ with end attachments for loading

The airframe sections-I & II are made of aluminium alloy AA 2014 in T6 condition which is a widely used light weight high strength aerospace material for flight structures and the fasteners are made of high strength EN24 steel. The mechanical properties of AA2014-T6, EN24 and C40 material utilised for the design and analysis are given in Table 5.1. The properties are obtained from tensile tests of three tensile specimens conducted in accordance to ASTM-E8 [53].

Table 5.1. Mechanical properties of materials in FIJ

Material	Young's Modulus E (GPa)	UTS σ_u(MPa)	0.2% proof strength σ_y(MPa)	% Elongation
AA2014-T6	61.1	447.2	312	10.2
EN24 Steel	187.6	1221.9	1084	18.4
C40 Steel	200.0	460.0	250	25.0

As the airframes are generally designed to limit the loads within 20% of the load corresponding to the first yield moment of the airframe, the lateral load to be applied on the experimental specimen is accordingly calculated.

5.2.2 Analysis of experimental setup

The geometric model of the tension type FIJ is analysed by importing the solid model to a FEA software ANSYS workbench [54]. The Section-I airframe and loading ring is discretised using hexahedral 20 node element with an element size of 2mm. The Section-II airframe is discretised using hexahedral and tetrahedral dominant elements with a size of 1mm. All fasteners like studs, screws and nuts are discretised with an element size of 1mm. The joining surfaces are provided with a frictional contact with coefficient of friction of 0.2 between C40 steel to AA 2014 joints and 0.5 between AA 2014 joints. A total of 4631481 elements are generated after discretisation as shown in Fig. 5.2. The base of Section-II airframe is fixed and constrained in all degrees of freedom. A force of 48470 N is applied at a distance of 205mm from the plane of FIJ to simulate a bending moment of 9.93 kNm which is equivalent to 20% of the first yield moment for the airframe as full load. This load is applied incrementally in steps of 10% of the full load till the full load on the airframe is applied.

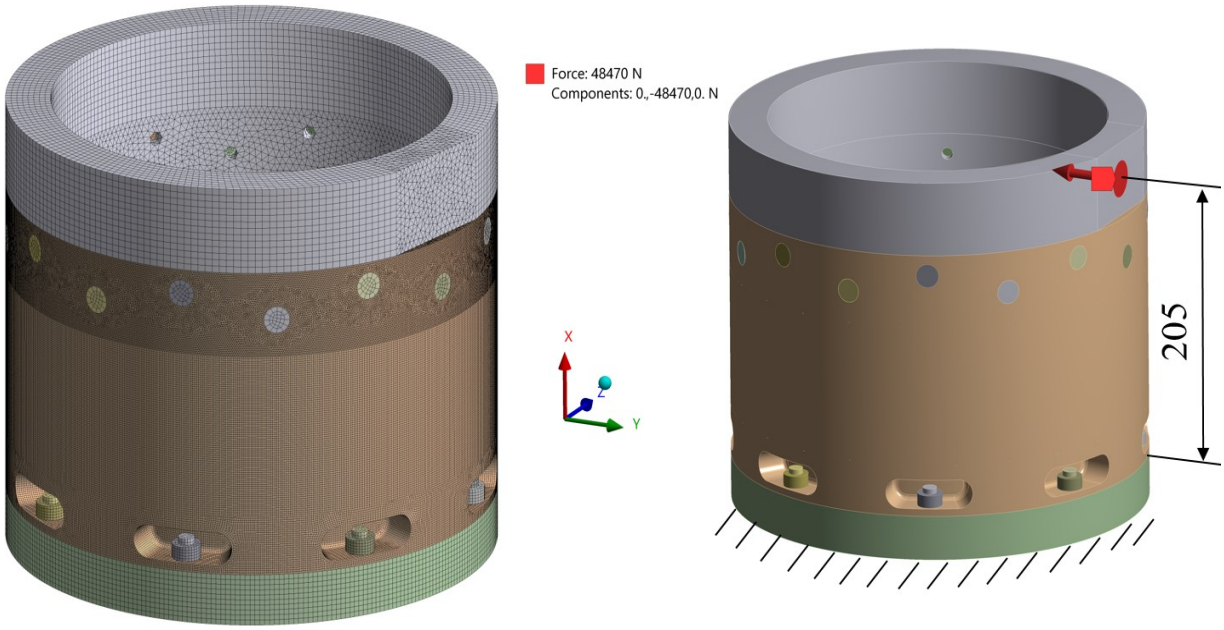

Fig. 5.2. FEA model of slot-nuttype FIJ for experiment

The maximum opening displacement at the joint along the circumference is determined due to the application of load. A maximum opening displacement of 0.422mm is obtained at the top reference in the joint as shown in Fig. 5.3. A plot of opening displacement variation along the airframe circumference is shown in Fig. 5.4.

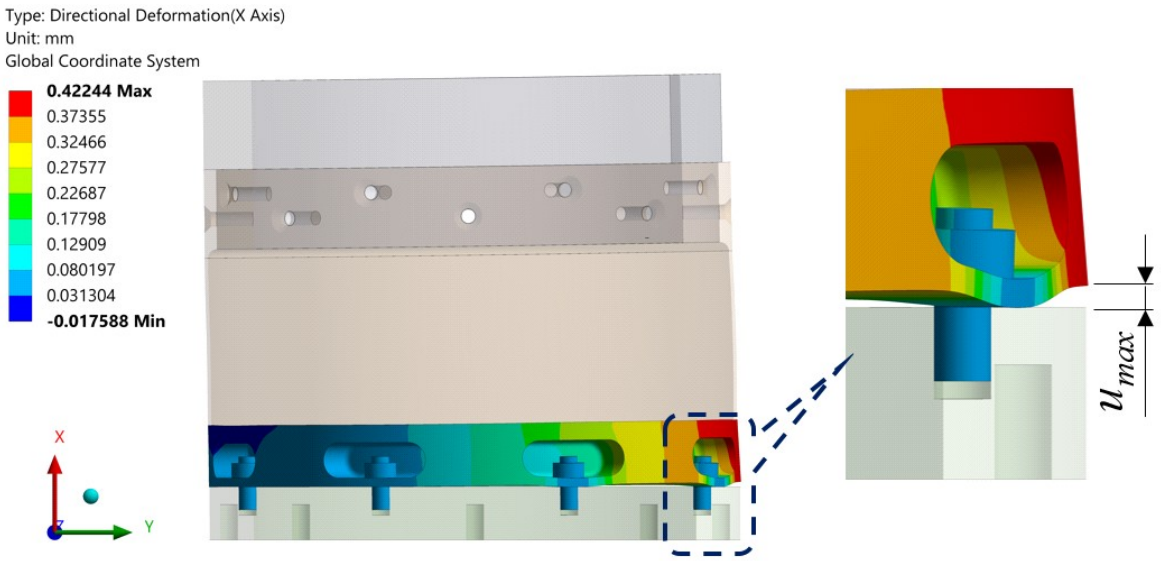

Fig. 5.3. Axial opening displacement in FIJ w.r.t. the plane of the FIJ

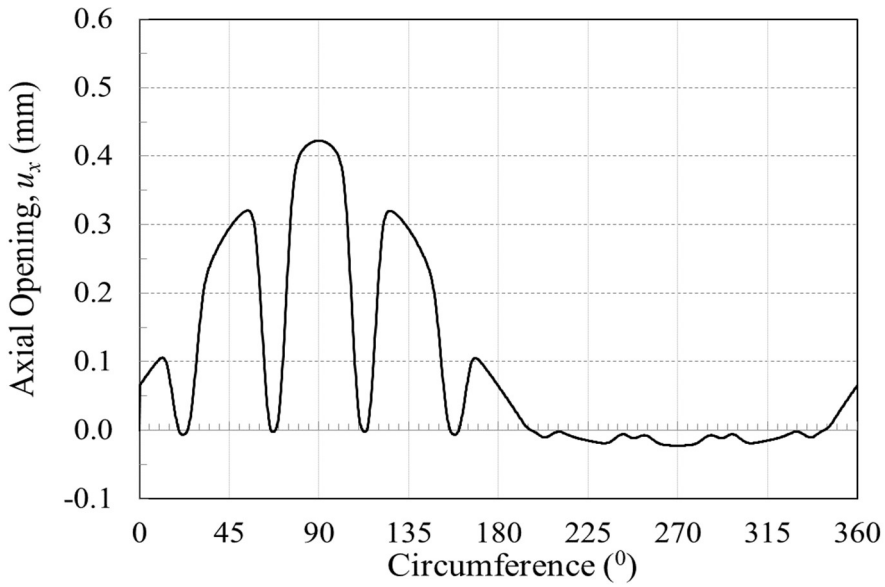

Fig. 5.4.Axial opening along circumference starting from RL at M/M_y =1

From the maximum joint opening, the joint opening angle is calculated in radians. This joint opening angle upon the applied bending moment results in the computation of the JRC in rad/Nm and the numerically computed JRC value for the chosen experimental setup of the FIJ is 0.241 rad/MNm.

5.3 Experimental Determination of JRC

The JRC is the characteristic property of a FIJ. The JRC determined numerically is validated by conducting the experiment.

5.3.1. Experimental setup

A detailed experimental configuration plan is evolved for the realisation of experimental set up. Four numbers of specimen FIJ as shown in Fig. 5.5(a) to (d) are manufactured to represent the actual setup as shown in Fig. 5.1. The raw material used for manufacture of the experimental specimens is in compliance with the aforementioned details. The fasteners adopted are EN24 material with 10.9 property class. The M10 studs are fastened to the Section-II airframe bulkhead and locked using a thread sealant Loctite 270 cured for 24 hrs. The Section-I and II airframes are assembled by introducing the studs in Section-II to pass through the receiving hole in the pockets/slots in the rear bulkhead of Section-I airframe and torque tightened with M10 nuts of property class 10.0 and torqued to 40Nm. The loading ring attachment is assembled to the front part of Section-I airframe with 12 numbers of M8 CSK screws and torqued to 20 Nm.The Section-II airframe is joined to the base plate using 12 numbers of M8 hexagonal socket head cap screws. A small L-shaped curved bracket is assembled to the rear bulkhead of Section-I airframe for placement of LVDT for measuring the joint opening while loading. The manufactured FIJ assembly for conducting the experiment is shown in Fig. 5.5(d). All the M10 studs used in the FIJ are torqued to 40Nm and M8 fasteners are torqued to 20Nm.

(a) Loading Ring

(b) Section-I Airframe

(c) Section-II Airframe

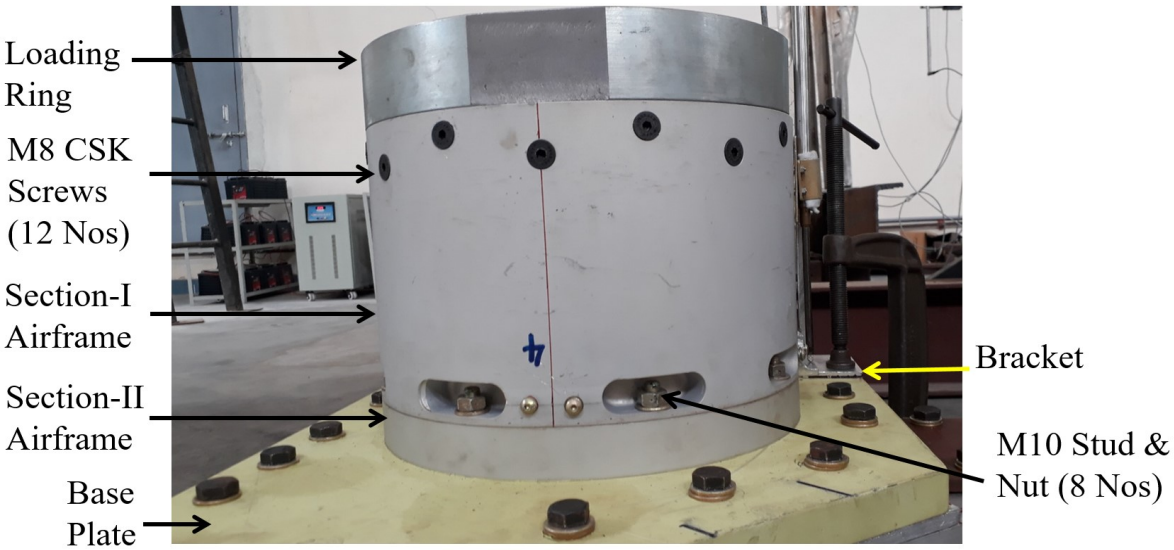

(d) Assembly of experimental FIJ specimen

Fig. 5.5. Details of realised experimental FIJ specimen

The above complete airframe assembly with FIJ is assembled to a rigid support structure made of ISHC structural steel at one end using the base reaction plate and C-channels on either sides. A hydraulic actuator with a capacity of 10 tons is assembled to an actuator mounting fixture using 4 numbers of M24 bolts on the right end. This assembly is mounted to the support structure at the other end using two L-brackets on either sides and rigidly clamped to the support structure with M12 bolts. An experimental test rig with motor and pump for supplying pressurised hydraulic fluid to the actuator cylinder is used for applying the lateral load on the specimen FIJ assembly. The configured experimental test set up is shown in Fig. 5.6 and its manufactured and assembled version is shown in Fig. 5.7. A total of four experimental specimens were manufactured and four different experiments were carried out. During experiments, for every increment of loading, the joint opening is measured using linear variable differential transducer (LVDT).

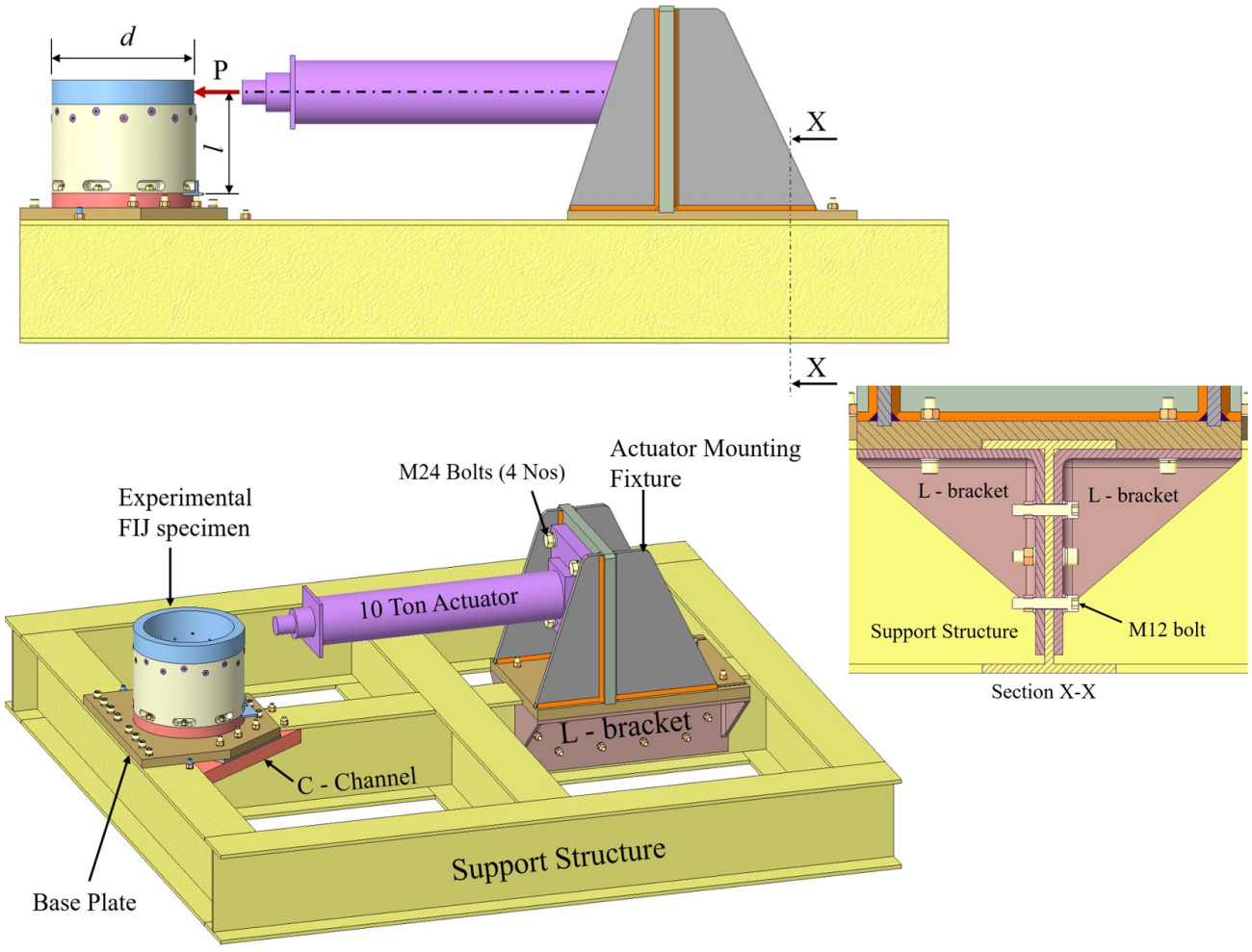

Fig. 5.6. Configuration details of the experimental setup

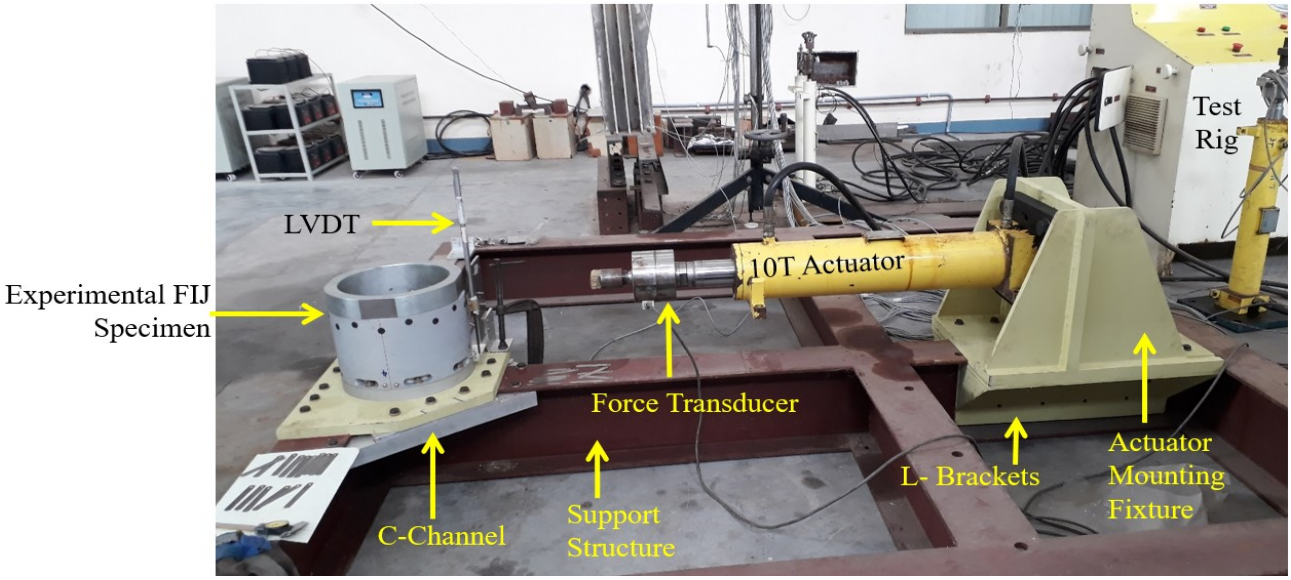

Fig. 5.7. Actual experimental setup

5.3.2 Instrumentation plan

A fool proof instrumentation plan with calibrated measuring devices are essential to obtain the true data during the experiment. The application of load on the loading ring of airframe assembly is by using a 10 Ton hydraulic actuator. The applied load is ensured by using a force transducer of HBM make U2B load cell model with a capacity 100kN. This load cell is assembled to the loading end of the actuator to monitor and control the applied load through a hydraulic power pack from the test rig. The joint opening is measured at the maximum tension side using a LVDT of HBM make WA-T/100mm model. The maximum deflection measurement of LVDT capacity is upto 100mm.The load cell and the LVDT is connected to data acquisition system for monitoring and recording the load and opening displacement. The instrumentation details constitute a NI based data acquisition system, load cell and LVDT employed in the experiments are shown in Fig. 5.8(a) to (c).

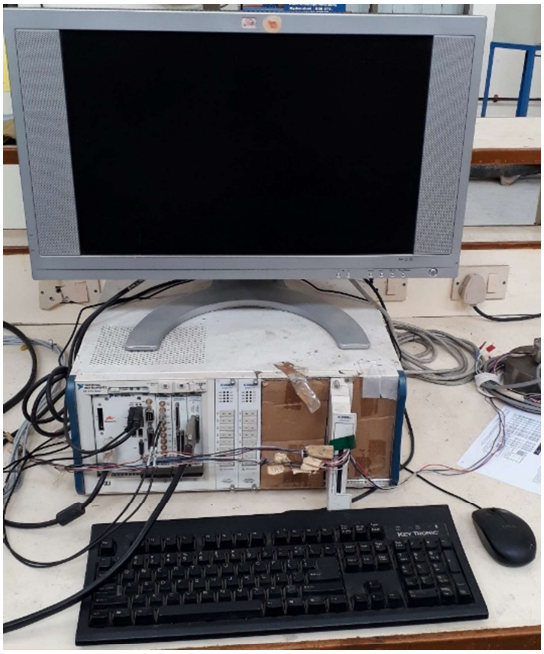

(a) NI based Data Acquisition System

(b) Force Transducer HBM U2B 100kN make

(c) LVDT HBM WA-T/100mm make

Fig. 5.8. Instrumentation details

5.3.3 Experiment and measurement of joint opening

The experiment is carried out by applying the lateral force through the hydraulic actuator. The load is increased incrementally for every 2500 N upto a maximum load of 48470 N to simulate the 20% of the first yield bending moment of the airframe. This load is applied at a distance of 205 mm from the airframe FIJ plane. The opening displacement at the slot-nut FIJ is measured using HBM based LVDT mounted to a L angle mounting bracket. Initially, the LVDT tip is made to contact with FIJ's attached bracket surface as shown in Fig. 5.9. The LVDT's initial displacement is set to zero prior to the application of load. The opening displacement is measured for every increment of loading i.e. in steps of 2500 N.

The opening displacement is converted to opening angle by dividing it with the radius of FIJ. The ratio between the opening angle and the applied bending moment provides the experimentally determined JRC for the FIJ. This experiment is repeated for additional three experimental specimens of FIJ. The results of experimentally determined JRC from four experiments is 0.22 rad/MNm as shown in Fig. 5.10.

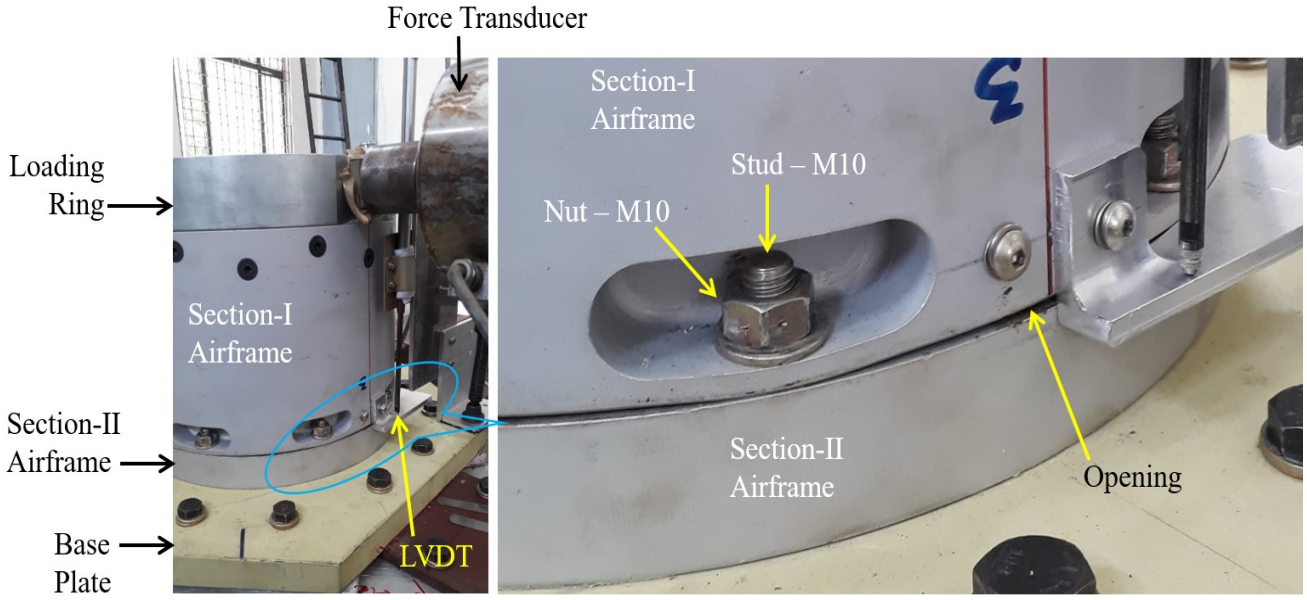

Fig. 5.9. Measurement of joint opening in experiment

5.4 Comparison of JRC Predictions with Experiments

The JRC obtained from the theory, numerical and experimental results are compared and shown in Fig. 5.10, where a good agreement is observed between experimental results and predictions from theoretical and numerical models. The experimental results of four experiments conducted on four different intersection joint specimens exhibit a small scattering around the theoretical predictions. On the other hand, numerical results found to show a slowly increasing trend with increase in loading which might be due to slight increase in flexibility of the FIJ when loading reaches close to the yield value of the material of FIJ. The reasonably good comparison between all three results demonstrate that the numerical model can be adopted confidently for prediction of JRC of the FIJ.

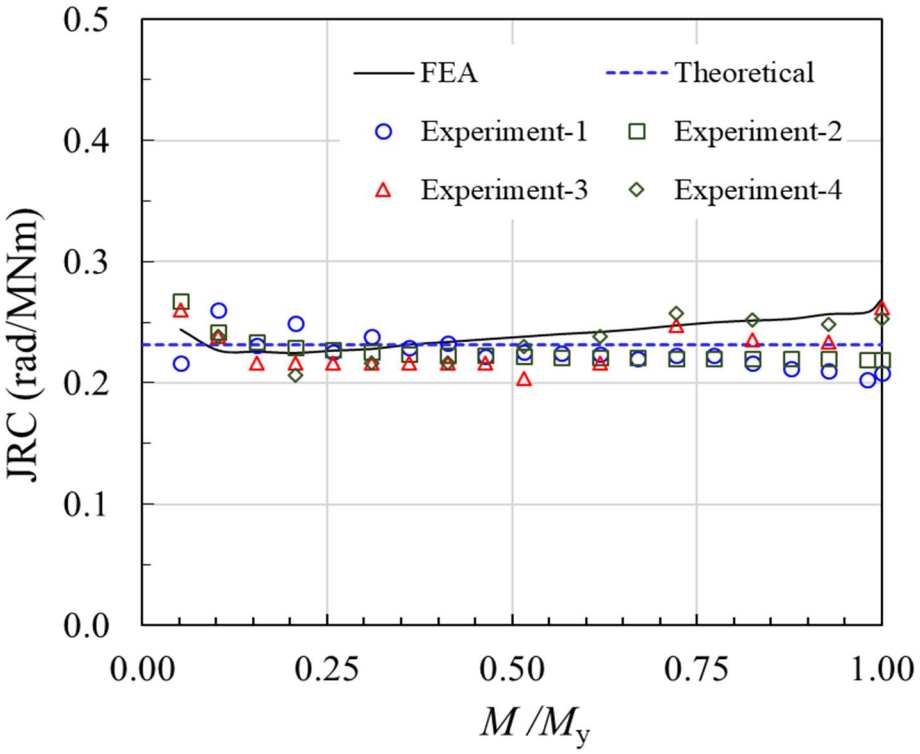

Fig. 5.10. Comparison of JRC between theory, numerical and experimental results

5.5 Summary

The JRC of the full FIJ has been measured through a specifically designed experimental setup. All the components required for the experimental FIJ specimens are designed and analysed before releasing the drawings for manufacturing. The ground support structure and fixtures are realised for carrying out the experiment and to ensure proper fixity to the base of the FIJ specimen and also for the loading attachments. The load corresponding to the first yield moment was applied incrementally through the load-controlled force transducer. The joint opening is measured at the FIJ interface plane through LVDT connected to a data acquisition system. The JRC thus obtained from experimental joint openings for all four FIJ specimens has shown appreciably good agreement with numerical predictions. These experiments validate the accuracy of the numerical model which in turn can be easily adopted to calculate the JRC of tension type FIJ for any airframe diameters.

Chapter – 6

Conclusion and Future Work

6.1 Conclusions

Stud-pocket tension type of FIJs play a vital role in ensuring the structural integrity of the launch vehicle. This research has provided theoretical model and numerical method to compute JRC and validated by experiments. The following conclusions can be drawn from the thesis.

i. JRC is a structural property of a FIJ and its prediction helps accurate modeling of a flight vehicle for dynamic characteristics.

ii. Local component joint stiffness of an FIJ is 14.0kN/mm from numerical and 13.8kN/mm from the experiment which are in close agreement thereby validating its adoption in theoretical model.

iii. Pre-tightening of studs enhances the JRC to an extent of 30% to 10% when loading is increased from no load to the first yield moment.

iv. Increase in number of studs for a given stud size could enhance the JRC significantly as compared to the increase in metric size of studs for the given number of studs.

v. The JRC is enhanced (ideal requirement) by increasing the inside pocket thickness, whereas the inside diameter for usage reduces resulting in integration difficulties.

vi. Higher numbers with lesser size of stud has enhanced JRC when compared with less numbers of higher sizes of studs. Hence, the FIJs with more number of studs are recommended when compared with lesser number of studs for the same stud size.

vii. Increasing the number of studs with increase in airframe diameter enhances the JRC of the FIJ.

viii. JRC is almost constant irrespective of any increase in applied bending moment within the yield limit.

ix. The JRC of full FIJ is 0.23 rad/MNm (theoretical model), 0.24 rad/MNm (numerical), and 0.22 rad/MNm (experiment) which are in good agreement. Hence, the numerical and /or theoretical method can be adopted for the computation of JRC for any diameter of FIJ.

x. This research helps in accurately predicting JRC of a tension-type of FIJ thereby eliminating the need for a detailed experimentation; and helps the designer to find accurate modal frequencies of the FIJ saving cost and time.

6.2 Future Work

Considerable research can be made in future as a continuation of this thesis. These are summarised below.

i. Four FIJs have been experimented. Additional FIJs may be experimented to obtain more results of JRC.
ii. Conducting compression loading on localized joint is challenging due to local buckling of airframe shell. This can be overcome with a special attachment.
iii. Determining local component joint stiffness rely on FEA or experiment. This dependency must be avoided and a method should be developed to compute the local joint stiffness theoretically so that the model becomes fully theoretical.
iv. Effect of fastener relaxation over time on JRC of an FIJ can be studied.
v. Experiments can be repeated for higher diameters of FIJ to ensure correctness of characterisation studies reported in thesis.

References

1. J.G. Maloney, M.T. Shelton, D.A. Underhill*, Structural dynamic properties of tactical missile joints -Phase 1*, General Dynamics, Pomona Division Report No.CR-6-348-945-001, (June 1970).
2. M. Umakanth, V. Narayanamurthy, S. Korla, A review of flight intersection joints, *International Journal of Reviews in Aerospace Engineering* (IREASE), 2021, 14(3): pp 131-148. https://doi.org/10.15866/irease.v14i3.19401 (Scopus)
3. J.G. Maloney, M.T. Shelton, *Structural dynamic properties of tactical missile joints-Phase 2*, General Dynamics, Pomona Division Report No. CR-6-348-945-002, (Sept 1971).
4. W. Hillmer, *Joint lock for thin walled cylinders*, US Patent 3100121, (1963).
5. G. Lasker, J. G. Maloney, M. T. Shelton, D. A. Underhill, *Structural dynamic properties of tactical missile joints-Phase 3*, General Dynamics, Pomona Division Report No. CR-6.348-945-003, (May 1974).
6. S. M. Gharouni, H.M. Panahiha, J.E. Jam, Space shuttle solid rocket motor (SRM) field joint: review paper, *Met. Mater. Eng.*, 20 (3), (2014), 155-163. https://doi.10.5937/metmateng1403155G.
7. K.C. Rockey, D.W. Griffiths, The behaviour of bolted flanged joints in tension, *Proc. of the Conference on Joints in Structures*, University of Sheffield, England, (1970).
8. *Bolted tension flange joint research (ring flanges joining CHS),* British Steel Corporation Tubes Division, Research Report CE 71/46, Corby, UK, (1974).
9. *BS 8100 Lattice towers and masts*, British Standards Institution, London, UK, (1988).
10. *Hollow structural sections design manual for connections*, 2nd Ed., Stelco Design Manual, Hamilton, Canada, (1981).
11. S. Igarashi, K. Wakiyama, K. Inoue, T. Matsumoto, Y. Murase, Limit design of high strength bolted tube flange joints (Part 1), *J. of Struct. & Const. Eng., Trans. of A.I.J.*, 354, (1985), 52-66.
12. S. Igarashi, K. Inoue, T. Matsumoto, Limit design of bolted circular tube flange joint subjected to tension, *Proc of the Int. Conference on Steel and Aluminium Structures*, Cardiff, UK, (1987), 825-834.
13. B. Kato, R. Hirose, Bolted tension flanges joining circular hollow section members, *Journal of Constructional Steel Research*, 5(2), (1984), 79-101.
14. CIDECT13, *Construction with hollow steel sections*, British Steel Corporation, Corby, UK, (1984).

15. J.A. Packer, J.E. Henderson, *Design guide for hollow structural section connections*, Canadian Institute of Steel Construction, Toronto, Canada, (1992).
16. J. J. Cao, A.J. Bell, Finite element analysis of circular flange joints under tension forces, *Proc. of 9th UK ABAQUS User Group Conference*, Exeter College, Oxford, UK, (1994).
17. J. J. Cao, A.J. Bell, Determination of bolt forces in a circular flange joint under tension force, *Int. J. Pres. Ves. & Piping*, 68 (1), (1996), 63-71. https://doi.org/10.1016/0308-0161 (95)00040-2.
18. J. J. Cao, A.J. Bell, Experimental study of circular flange joints under tension forces, *Journal of Strain Analysis for Engineering Design,* 31(4), (1996), 259-267. https://doi.org/10.1243/03093247V314259.
19. J. J. Cao, J.A. Packer, Design of tension circular flange joints in tubular structures, *Engineering Journal*, *First Quarter*, (1997), 17-23.
20. G. Stamatopoulos, J. Ermopoulos. Interaction curve for non-preloaded bolted connections in tubular members, *Proc. of Eurosteel 2008, 5th Conference on Steel and Composite Structures*, Graz, Austria, (2008), 27-35.
21. M. Couchaux, M. Hjiaj, I. Ryan, Static resistance of bolted circular flange joints under tensile force, *Proc. 13th Int. Symposium on Tubular Structures*, Hong-Kong, (2010). doi: 10.1201/b10564-6.
22. M. Couchaux, M. Hjiaj, I. Ryan, Behaviour of bolted circular flange joints subjected to a bending moment and an axial force, *Proc. of Eurosteel* 2011, *5th Conference on Steel and Composite Structures*, Budapest, Hungary, (2011), 219-224.
23. A.Wojnar, A. Kozłowski, Mechanical model for assessment of the stiffness of bolted flanged joint, *Proc. of the 11th Int. Conf. on Metal Structures*, Taylor & Francis, Rzeszów, Poland, (2006), 188-189.
24. A. Kozlowski, A. Wojnar, L. Sleczka, Influence of flanged bolted joints stiffness on the behaviour of steel chimneys, *Proc. of the 3rd Int. Conference on Structural Engineering*, Mechanics and Computation, Cape Town, South Africa, (2007).
25. A. Kozlowski, A. Wojnar, Initial stiffness of flange bolted joints and their influence on the behaviour of steel chimneys, *Proc. of Eurosteel 2008, 5th Conference on Steel and Composite Structures*, Graz, Austria, (2008).
26. M.R. Azim, An analytical investigation on bolt tension of a flanged steel pipe joint subjected to bending moments, *Int. J. of Eng. and App. Sci*., 2(3), (2013).
27. M. Emara, E.S. Ahmed, E. Soliman, A. Azhar, Numerical analysis of CHS unstiffened bolted circular flange connection, *University Civil Eng. Res. Magazine*, 41 (1), (2019).

28. V. Weissberg, K. Wander, R. Itzhakov, A new approach to load transfer in bolted joints, 1988, *Proc. of the Int. Council of Aeronautical Sciences*, Israel Aircraft Industries Ltd, AIAA and ICAS-88-3.1.4 (1988), 96-101.
29. C.T. Allen. *Computation of bolted joint stiffness using strain energy*, Master of Science Thesis, University of Alabama, (2003).
30. O. Zhang, J.A. Poirier, New analytical model of bolted joints, *ASME J. of Mech. Des*., 126(4), (2004), 721-728. https://doi.org/10.1115/1.1760777.
31. I.R. Grosse, L.D. Mitchell, Nonlinear axial stiffness characteristics of axisymmetric bolted joints, *ASME J. of Mech. Des*., 112(3), (1990), 442-449. https://doi.org/10.1115/1.2912628.
32. R.K. Roy, *Design and behavior of bolted joints*, Nutek Inc, Version: 0602, (2014).
33. J. Kim, J.C. Yoon, B.S. Kang, Finite element analysis and modelling of structure with bolted joints, *J. of App. Math. Modelling*, 31(5), (2006), 865-911. https://doi.org/10.1016/j.apm.2006.03.020.
34. J. Montgomery, *Methods for modelling bolts in the bolted joint*, Siemens, Westinghouse Power Corporation, Orlando, FL, USA, (2002).
35. T.F. Lehnhoff, B.A. Bunyard, Effects of bolt threads on the stiffness of bolted joints, *ASME J. Pre. Ves. Tech*., 123(2), (2001), 161-165. https://doi.org/10.1115/1.1319504.
36. J. Wileman, M. Choudhury, I. Green, Computation of member stiffness in bolted connections, *ASME J. of Mech. Des*., 113(4), (1991), 432-437. https://doi.org/10.1115/1.2912801.
37. N. Rasti, Comparative study of joint stiffness calculations using finite element analysis, M.S. Thesis, University of Windsor, Canada, (2007).
38. S.A. Nassar, X. Yang, S.V.T. Gandham, Z. Wu, Nonlinear deformation behavior of clamped bolted joints under a separating service load, *J. of Pres. Ves. Tech., 133(2)*, (2011), 1-9. https://doi.org/10.1115/1.4002674.
39. G.M. Henson, B.A. Hornish, An evaluation of common analysis methods for bolted joints in launch vehicles, *AIAA Journal*, 3022, (2010), 1-27. https://doi.org/10.2514/6.2010-3022.
40. N. Kumar, P.V.G. Brahamanandam, B.V.P. Rao, 3-D finite element analysis of bolted flange joint of pressure vessel, *MIT Int. J. of Mech. Eng.,* 1(1), (2011), 34-39.
41. S.M. Kaplan, Flexibility coefficients for structural joint assemblies, *J. of Spacecrafts and Rockets*, 8(1), (1971), 76-77. https://doi.org/10.2514/3.30223.

42. B. Kumar, N.V.M. Rao, R.K. Gupta, J.R. Mohan, Prediction and measurement of free vibration response of multistage launch vehicles, *Proc. of 1st Indian Conference on Applied Mechanics* (INCAM-2013), IIT Madras, (2013), 1-6.
43. J.B. Gunda, Y. Krishna, Influence of joint flexibility on vibration analysis of free-free beams. *Nonlinear Engineering*, 3(4), (2014), 237–246. https://doi.org/10.1515/nleng-2014-0012.
44. V.L. Alley, A.H. Gerringer, *A matrix method for the determination of the natural vibrations of free-free unsymmetrical beams with applications to launch vehicles*, NASA TN D-1247 (1962).
45. S.A. Leadbetter, V.L. Alley, W.H. Robert, A.H. Gerringer, *An experimental and analytical investigation of the natural frequencies and mode shapes of a four stage solid propellant rocket vehicle*, NASA Technical Note D – 1354, (Aug 1962).
46. V.L. Alley, S.A. Leadbetter, The prediction and measurement of natural vibrations on multi stage launch vehicles, *AIAA Journal*, 1(2), (1963), 374-379. https://doi.org/10.2514/3.1540.
47. R. Newlands, M. Heywood, A. Lee, *Rocket vehicle loads and airframe design*, ASPIRE Space, Technical paper, (2012).
48. www.Military-Today.com
49. www.quickgs.com/list-of-indian-missiles-with-range/
50. Ammunition handling equipment, 14313B_Ch09, http://www.navybmr.com/study%20material/NAVEDTRA%2014313B/14313B_ch09.pdf.
51. C. Roberts. D. Ewins, Multi-axis vibration testing of an aerodynamically excited structure, *J. of Vib. & Control*, 24(2), (2016), 427-437. https://doi.org/10.1177/1077546316642064.
52. K.L. McIntyre, *Modified Holzer-Myklestad model analysis*, Final Report - CWA 245, General Dynamics, Pomona Division, Report No. TM 348-15, (July 1961).
53. ASTM E8/E8M-13, Standard Test Methods for Tension Testing of Metallic Materials, Aug 2013, DOI: 10.1520/E0008_E0008M-13A.
54. ANSYS Workbench User's Manual. Version 18.1. ANSYS Corporation Inc., USA. 2019.